VTRC
Virginia Transportation
Research Council

Evaluation of Fatigue-Prone Details Using a Low-Cost Thermoelastic Stress Analysis System

http://www.virginiadot.org/vtrc/main/online_reports/pdf/17-r8.pdf

STEVEN B. CHASE, Ph.D.
Research Professor

YAW ADU-GYAMFI, Ph.D.
Research Associate

Department of Civil and Environmental Engineering
University of Virginia

Final Report VTRC 17-R8

VIRGINIA TRANSPORTATION RESEARCH COUNCIL
530 Edgemont Road, Charlottesville, VA 22903-2454
www.VTRC.net

Standard Title Page - Report on Federally Funded Project

1. Report No.: FHWA/VTRC 17-R8	2. Government Accession No.:	3. Recipient's Catalog No.:
4. Title and Subtitle: Evaluation of Fatigue-Prone Details Using a Low-Cost Thermoelastic Stress Analysis System		5. Report Date: November 2016 6. Performing Organization Code:
7. Author(s): Steven B. Chase, Ph.D., and Yaw Adu-Gyamfi, Ph.D.		8. Performing Organization Report No.: VTRC 17-R8
9. Performing Organization and Address: University of Virginia 351 McCormick Road Charlottesville, VA 22904		10. Work Unit No. (TRAIS): 11. Contract or Grant No.: 103658
12. Sponsoring Agencies' Name and Address: Virginia Department of Transportation 1401 E. Broad Street Richmond, VA 23219 Federal Highway Administration 400 North 8th Street, Room 750 Richmond, VA 23219-4825		13. Type of Report and Period Covered: Final Contract 14. Sponsoring Agency Code:
15. Supplementary Notes:		

16. Abstract:

This study was designed to develop a novel approach for in situ evaluation of stress fields in the vicinity of fatigue-prone details on highway bridges using a low-cost microbolometer thermal imager.

The method was adapted into a field-deployable instrument to obtain in situ visualization of the stress concentrations present at fatigue-prone details on highway bridges subject to random truck loading. The infrared thermoelastic stress analysis (IR-TSA) system developed in this study is available for use by Virginia Department of Transportation (VDOT) district structure and bridge personnel to evaluate fatigue-prone details on existing bridges.

VDOT plans to implement the technology to validate repairs underway at the I-64 Delta Frame Bridge in Lexington and fatigue crack arrest repairs on other steel bridges in VDOT's inventory. Guidance will be developed on the application and practical use of the technology for incorporation into VDOT's Manual of the Structure and Bridge Division.

17 Key Words: Bridges, structural steel, fatigue-prone details, infrared thermography		18. Distribution Statement: No restrictions. This document is available to the public through NTIS, Springfield, VA 22161.	
19. Security Classif. (of this report): Unclassified	20. Security Classif. (of this page): Unclassified	21. No. of Pages: 51	22. Price:

Form DOT F 1700.7 (8-72) Reproduction of completed page authorized

FINAL REPORT

EVALUATION OF FATIGUE-PRONE DETAILS USING A LOW-COST THERMOELASTIC STRESS ANALYSIS SYSTEM

Steven B. Chase, Ph.D.
Research Professor

Yaw Adu-Gyamfi, Ph.D.
Research Associate

Department of Civil and Environmental Engineering
University of Virginia

VTRC Project Manager
Michael C. Brown, Ph.D., P.E., Virginia Transportation Research Council

In Cooperation with the U.S. Department of Transportation
Federal Highway Administration

Virginia Transportation Research Council
(A partnership of the Virginia Department of Transportation
and the University of Virginia since 1948)

Charlottesville, Virginia

November 2017
VTRC 17-R8

DISCLAIMER

The reported project was performed under contract for the Virginia Department of Transportation, Virginia Transportation Research Council. The contents of this report reflect the views of the authors, who are responsible for the facts and the accuracy of the data presented herein. The contents do not necessarily reflect the official views or policies of the Virginia Department of Transportation, the Commonwealth Transportation Board, or the Federal Highway Administration. This report does not constitute a standard, specification, or regulation. Any inclusion of manufacturer names, trade names, or trademarks is for identification purposes only and is not to be considered an endorsement.

Each contract report is peer reviewed and accepted for publication by staff of Virginia Transportation Research Council with expertise in related technical areas. Final editing and proofreading of the report are performed by the contractor.

ABSTRACT

This study was designed to develop a novel approach for in situ evaluation of stress fields in the vicinity of fatigue-prone details on highway bridges using a low-cost microbolometer thermal imager.

The method was adapted into a field-deployable instrument to obtain in situ visualization of the stress concentrations present at fatigue-prone details on highway bridges subject to random truck loading. The infrared thermoelastic stress analysis (IR-TSA) system developed in this study is available for use by Virginia Department of Transportation (VDOT) district structure and bridge personnel to evaluate fatigue-prone details on existing bridges.

VDOT plans to implement the technology to validate repairs underway at the I-64 Delta Frame Bridge in Lexington and fatigue crack arrest repairs on other steel bridges in VDOT's inventory. Guidance will be developed on the application and practical use of the technology for incorporation into VDOT's *Manual of the Structure and Bridge Division.*

FINAL REPORT

EVALUATION OF FATIGUE-PRONE DETAILS USING A LOW-COST THERMOELASTIC STRESS ANALYSIS SYSTEM

Steven B. Chase, Ph.D.
Research Professor

Yaw Adu-Gyamfi, Ph.D.
Research Associate

Department of Civil and Environmental Engineering
University of Virginia

INTRODUCTION

The Virginia Department of Transportation (VDOT), like all state departments of transportation, is responsible for ensuring the safe performance of the transportation network under its jurisdiction. The bridges on these highways are essential parts of this network and must be kept functioning safely within policy and budget constraints. One recurring problem on bridges with steel superstructures is that some of these bridges contain structural details that are prone to fatigue or distortion-induced cracking. These cracks can grow to critical size and can lead to brittle fracture and result in greatly reduced load capacity and even collapse of the bridge. Through experience, state departments of transportation are generally aware of the problem and know where these cracks are likely to occur. Consequently, the current state of practice is to visually inspect these details for the presence of cracks. Such inspections require close-up visual access to the details and are time-consuming. In addition, a crack could form that is difficult to observe by conventional inspection methods and may remain undetected for some time. The current study develops and delivers a relatively inexpensive device that greatly increases the reliability of prediction, detection and monitoring of fatigue cracks. This new device will be useful for characterizing and evaluating stress concentrations on steel structures both in the laboratory and in the field. Another very promising use of this new device will be to evaluate the effectiveness of repairs or retrofits in eliminating stress concentrations.

The device developed relies on an emerging non-contact, non-destructive evaluation technique. The device employs the principles of Thermoelastic Stress Analysis (TSA) to visualize the full-field stress field under dynamic loading. TSA maps the stress state of a structure or element of a structure by capturing any temperature changes on its surface while being subjected to dynamic strains due to transient loads, most likely due to moving vehicles (trucks). However, resolving a full-field stress solution requires significant post-processing of the acquired temperature change data.

It is well known that an object experiences a change in temperature as it undergoes deformation. The change in temperature is due to two main effects: thermoelasticity and elastoplasticity. Elastoplasticity-induced temperature changes are due to energy dissipation in

the object caused by internal friction resulting in mechanical energy to be converted into heat. It produces a temperature gain, which can be related to the load amplitude, frequency and duration. This temperature gain occurs regardless of loading direction. Thermoelasticity, on the other hand, is explained by the first law of thermodynamics, which states that an object subjected to mechanical stress undergoes a change in volume, which in turn causes a variation in the object's temperature. The temperature change produced by thermoelasticity is synchronous to the loading history and is also proportional to the amplitude of the load (Zanetti et al., 2007). Additionally, it is also proportional to the amplitude of the first stress invariant (sum of the principal stresses) and is therefore useful for stress analysis. Compared to elastoplasticity, thermoelasticity produces a very small temperature change. A primary goal of post-processing the captured temperature change data is to isolate the thermoelasticity-induced temperature change response contribution.

TSA has been successfully applied by major industries in engineering and medical sciences for damage detection, fatigue monitoring and validation of design concepts (Emery and Dulieu-Barton, 2010; Freuhmann et al., 2010; Patki and Pratterson, 2010; Diaz et al., 2013; Haldorsen, 1998). An extended application of TSA is to analyze the stresses of fatigue-prone structural details of steel bridges in situ. This application is complicated and not direct for several reasons. Conventional applications of TSA technology rely on very bulky, heavy and expensive photonic cameras, as shall be described later. Consequently, these cameras are impractical for field use on steel bridges. Also, current TSA technologies have generally relied on well-defined cyclical loading, typically sinusoidal. This imposed loading restriction limits this technology's applicability to well-controlled loading conditions. Consequently, it is very challenging to use TSA under service loading conditions in the field, which are mostly random and are unlikely to be cyclical. Although researchers foresaw the extension of TSA to loading that is variable-amplitude, non-cyclical and random (Harwood and Cummings, 1991; Greenee et al., 2008), very little has been done in this area (Freuhmann et al., 2010; Rajic and Rowlands, 2013).

PURPOSE AND SCOPE

The device and methodology developed in this study make it possible to perform a full-field TSA on a bridge component subjected to random transient stresses using low-cost infrared (IR) cameras. An IR-imaging device was developed that can be used to nondestructively identify [dynamic] stress concentrations in highway bridge details. The key components of the device include the following:

- a relatively low-cost (less than $6000) thermal imager that measures changes in the surface temperature of the component subjected to time-varying stresses, caused by transient loads

- signal processing software for analyzing and displaying acquired thermal images

- a dedicated field computer for housing signal-processing algorithms and data acquisition

- a sensor to detect random load presence and amplitude to trigger data acquisition.

This device is also capable of detecting and evaluating existing fatigue cracks by imaging the characteristic large stress concentration(s) of growing cracks. Using this device, bridge inspectors are able to locate and evaluate hard-to-observe cracks. This includes cracks beneath coatings. The effectiveness of crack-arresting maintenance actions can also be evaluated. Moreover, the device may be used to facilitate crack prevention as it detects large stress concentrations before cracks develop.

METHODS

Review of Thermoelastic Stress Analysis

Thermoelastic stress analysis is a non-contact, non-destructive evaluation technique used to acquire full-field stress data from the surfaces of materials or components. While this method has been successfully used for stress analysis for many years, this has been in manufacturing and laboratory setting and the method is unfamiliar to most bridge engineers. TSA uses IR detection to measure small changes in temperature induced by dynamic loads, of sufficient amplitude and frequency, and relates them to the associated dynamic stresses (Greenee et al., 2008). Although TSA provides data related to the first stress invariant, which is not directly related to failure, it should be noted that in many components, maximum stress occurs at the edges where only one stress exists (Dullieu-Barton, 1999).

Prior applications of TSA have been reported in major industries in engineering and medical sciences. In civil and mechanical structures, the technique has been used to investigate the fatigue properties of components and consequently for improved re-design of the structural components (Johnson, 2006). TSA also has the ability to resolve fine details in a component subjected to time varying stresses. Several authors have used this capability for detecting and monitoring cracks or anomalies in material components (Emery and Dulieu-Barton, 2010). In medical sciences and bio-engineering, the technique has been used to identify stress distributions for different types of bones in the human body such as the femur (Shah et al., 2012), pelvis (Zanetti et al., 2012) and patella (Friis et al., 1993). This provides useful information when designing replacements for these bones. Regions of high stress can be identified, redesigned or more material could be added to prevent failure.

Theory of TSA

Lord Kelvin in 1853 proposed that a material subjected to mechanical stress will experience a change in volume. This change in volume results in a corresponding change in the temperature of the material under stress. That is, a material's temperature rises if it is

compressed, whereas tension (expansion) produces a cooling effect. This general idea is fundamental to the development of the theory of TSA.

Assuming that a homogenous material is subjected to a linear elastic stress, the relationship between the resulting change in temperature and the stress in the material can be described by Equation 1:

$$\Delta T = \frac{T}{\rho C_\varepsilon} \sum \frac{\delta \sigma_{ij}}{\delta T} \varepsilon_{ij} + \frac{Q}{\rho C_\varepsilon} \quad \text{Eq. 1}$$

where

ΔT = *Change in temperature*
T = *Bulk absolute temperature of the material*
ρ = *Density*
C_ε = *Specific heat at constant strain*
σ_{ij} = *Stress change tensor*
ε_{ij} = *Strain change tensor*
Q = *Heat input.*

The second term in the equation is necessary when heat conduction takes place during the loading of the material. Heat conduction causes the temperature changes to be transitory, making the application of TSA challenging. This term can, however, be neglected if no heat conduction takes place within the material during the application of the loads. This is achieved by applying cyclic loads at a suitably high frequency. When adiabatic conditions (no heat conduction) are maintained, the change in temperature of the material's surface is proportional to the first stress invariant. Therefore, the expression in Equation 1 can be re-written as Equation 2:

$$\Delta T = \frac{\alpha T}{\rho C_\varepsilon} \Delta(\sigma_1 + \sigma_2) \quad \text{Eq. 2}$$

where

σ_1 *and* σ_2 = *Principal stresses*
α = *Linear coefficient of thermal expansion.*

It is reiterated that the expression above is valid only when the frequency of the applied load is high enough to assume adiabatic conditions. Increasing the loading frequency shortens the thermal diffusion length. The minimum loading frequency required to maintain adiabatic conditions for a material is, however, dependent on the thermal conductivity of the material and the stress gradients generated by the loading conditions (Harwood and Cummings, 1991). The loading frequency necessary for successful application of TSA to highway bridges was investigated during the laboratory portion of this study.

The variation in surface temperature is measured using IR detectors. The IR detectors produce a voltage output that corresponds to spectral radiant photon emittance(φ) from the surface of the material. The radiant photon emittance of a material is dependent on its temperature and is quantified by Equation 3:

$$\varphi = eBT^3 \quad \text{Eq. 3}$$

where

φ = *Spectral radiant photon emittance*
e = *Surface emissivity*
B = *Stefan-Boltzmann constant*
T = *Surface temperature (K).*

The change in photon emittance ($\Delta\varphi$) resulting from a change in temperature can therefore be represented in Equations 4 through 6 as follows:

$$\Delta\varphi = 3eBT^2\Delta T \quad \text{Eq. 4}$$

$$\Delta T = \left(\frac{\Delta\varphi}{3BT^2}\right) \times \left(\frac{1}{e}\right) \quad \text{Eq. 5}$$

Substituting ΔT into Equation 2,

$$\Delta(\sigma_1 + \sigma_2) = \left(\frac{\Delta\varphi}{3BT^2}\right) \times \left(\frac{1}{TeK}\right) \quad \text{Eq. 6}$$

where

$$K = \frac{\alpha}{\rho C_\varepsilon}$$

A linear relation between the output voltage from the IR detector and the change in photon emittance, $\Delta\varphi$, can be assumed. A constant ($A = 1/3BT^3eK$) that is dependent on the material properties, namely the coefficient of thermal expansion, density, specific heat capacity, surface emissivity and bulk absolute temperature, is calculated. Making these substitutions, Equation 6 can be re-written as Equation 7:

$$\Delta(\sigma_1 + \sigma_2) = A\Delta\varphi \quad \text{Eq. 7}$$

For this linear relationship to exist, photon emittance from the surface of the material must be uniform. The emissivity of the surface can be made uniform with the appropriate surface preparation, such as a thin and uniform coat of flat black paint. The black paint also provides low surface reflectivity, reducing unwanted reflections into the IR detector.

Technology of Infrared Cameras

A key component of the TSA system is the IR camera. These are designed to respond to IR radiation. In the context of TSA, surface temperatures change when material deformation occurs. As explained earlier, the magnitude of such temperature changes can be very small. Therefore, a sufficient IR camera requires very sensitive and [electronically] sophisticated

detectors. Then, when combined with appropriate signal post-processing, the thermoelastic effect, or change in stress, may be accurately calculated. There are two types of IR detectors that have been used for TSA:

1. photonic detectors
2. thermal detectors.

Photonic detectors contain narrow band-gap energy semiconductors, which generate an output voltage signal when excited by photons. These photons are emitted from the surface of heated objects as thermal radiation. The output signal from the detector is proportional to the rate of incident photons. Therefore, for photonic detectors to work optimally, the incident photons must have sufficient energy to excite the semiconductors. Photonic detectors are very sensitive, responsive and have ideal signal-to-noise performance characteristics. The sensitivity of IR cameras with photonic detectors is expressed by its noise equivalent temperature difference (NETD), which can be as low as 10 mK (milli-Kelvin). NETD is measured by noting the temperature difference between that target and the background for an incident signal that produces a signal-to-detector noise ratio of one. Photonic detectors work in the mid-wave IR spectral band, where wavelengths are much shorter ($3\mu m - 5\mu m$) than the long-wave band (FLIR). As a result, they are able to provide crisp, high-resolution images and superior thermal contrast (i.e., the change in signal for a change in target temperature). This is very important for backgrounds that may not be much colder or hotter than the target. However, a significant drawback is that these detectors require cooling to temperatures as low as 60 to 100 °K; this is required to reduce flooding or blinding of the sensor by its own thermal radiation. To achieve this, the detectors are integrated with liquid nitrogen baths or cryogenic coolers, in a vacuum-sealed case, which makes the detector bulky, heavy, expensive and sometimes inconvenient to use.

The first commercial IR camera system developed for TSA was the SPATE (Stress Pattern Analysis by Thermal Emission) system. The SPATE system uses a single photon emission detector for point-by-point scanning of an image with a pair of moveable mirrors. The detector was sensitive to radiation with wavelengths in the 8 to 14 μm range; in this range the thermoelastic effect is readily visible. Recent generations of photon emission detectors contain two-dimensional array detectors that do not require a raster scanning mechanism for acquiring images. These detectors are called focal plane array (FPA) detectors. FPA detectors provide higher spatial resolution, when compared to point-by-point scanning methods. Also, the FPA detectors are capable of recording thousands of data points concurrently; this is useful for monitoring transient events (Rogalski, 2002). The FLIR SC 7000 and GF 335 are typical examples of differential IR cameras with photonic detectors.

Thermal detectors, contrasted to photonic detectors, operate on the principle that when subjected to IR radiation, their temperature increases and the resulting change can be measured by any temperature-dependent mechanism, such as resistance, voltage, etc. and can be used to generate an electrical output. Bolometer detectors are resistance-based thermal detectors; the FLIR camera used in this investigation is a typical example of an IR camera using a microbolometer thermal detector. Since thermal detectors rely on the total amount of radiant energy reaching the detector, their response is generally independent of wavelength; rather, their

response depends on the rate of change of radiation (Ciupa and Rogalski, 1997). Thermal detectors are stabilized at ambient temperature; consequently, cryogenic coolers are not required. They are more sensitive to radiation in the long-wave IR band ($7\mu m - 14\mu m$). Compared to thermal detector cameras, photonic detector cameras are generally 2 to 3 times more sensitive. However, thermal detector cameras are much less expensive, smaller and very convenient to use. The recent generation of thermal imagers also contains two-dimensional array detectors that do not require a scanning mechanism for acquiring images.

Data Processing and Analysis

The output voltage from IR detectors contains signals due to incoming radiation. This includes the thermoelastic and thermos-plastic responses, as well as other inherent noises. From this point forward, inherent noises and the thermoplastic response shall be considered together and called noise. This is because only the thermoelastic response is of interest. For example, a steel specimen exposed to high cyclic stresses could produce a thermoelastic based output voltage response on the order of 0.020V in total amplitude (i.e., high-peak to low-peak); however, this response signal might be buried in the accompanying large-bandwidth noise that may be on the order of 0.800V (Harwood and Cummings, 1991). Isolating the thermoelastic information from the noisy output requires the application of sophisticated signal and image processing routines. Historically, there have been two primary approaches used to process IR image data. Although not used in the development of the device in this project, there is some benefit in understanding the classical applications of frequency filters and lock-in amplifiers.

Frequency Filters

Frequency filters are arguably the simplest way to detect a signal at a specific frequency in the presence of large background noise; they are popular because they are easy to design, and can work in real-time. Frequency filters are very useful for rejecting noise that is far away in frequency from the signal of interest. Low-pass and band-pass filters are the two most frequently used types of frequency filters in IR data processing. The low-pass filter allows all frequencies below a certain cut-off frequency to pass through. The band-pass filter allows only frequencies within a predefined frequency band to pass. Frequency filters work optimally when the signal of interest has a constant amplitude and frequency over time.

However, filters are not perfect; that is, they cannot allow signals of a selected frequency region to pass by completely free of distortion, nor can they completely reject signals at other frequencies. During filter design, the transition from a passing signal to a rejected signal is usually gradual (see Figure 1). Hence, frequencies outside the desired range are attenuated instead of being completely rejected. This introduces distortions into the final output. It is very challenging to use filters to process IR images generated by signals with random characteristics. They either smooth out the desired thermoelastic output or introduce noisy information into the desired output. Figure 2 illustrates an example of using a low-pass filter to process a noisy signal.

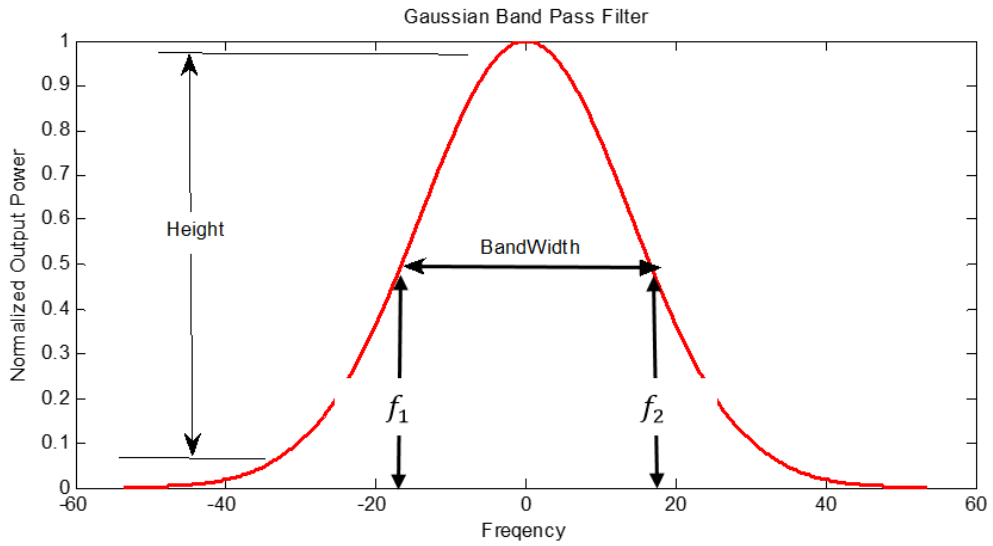

Figure 1. Typical Band-Pass Filter

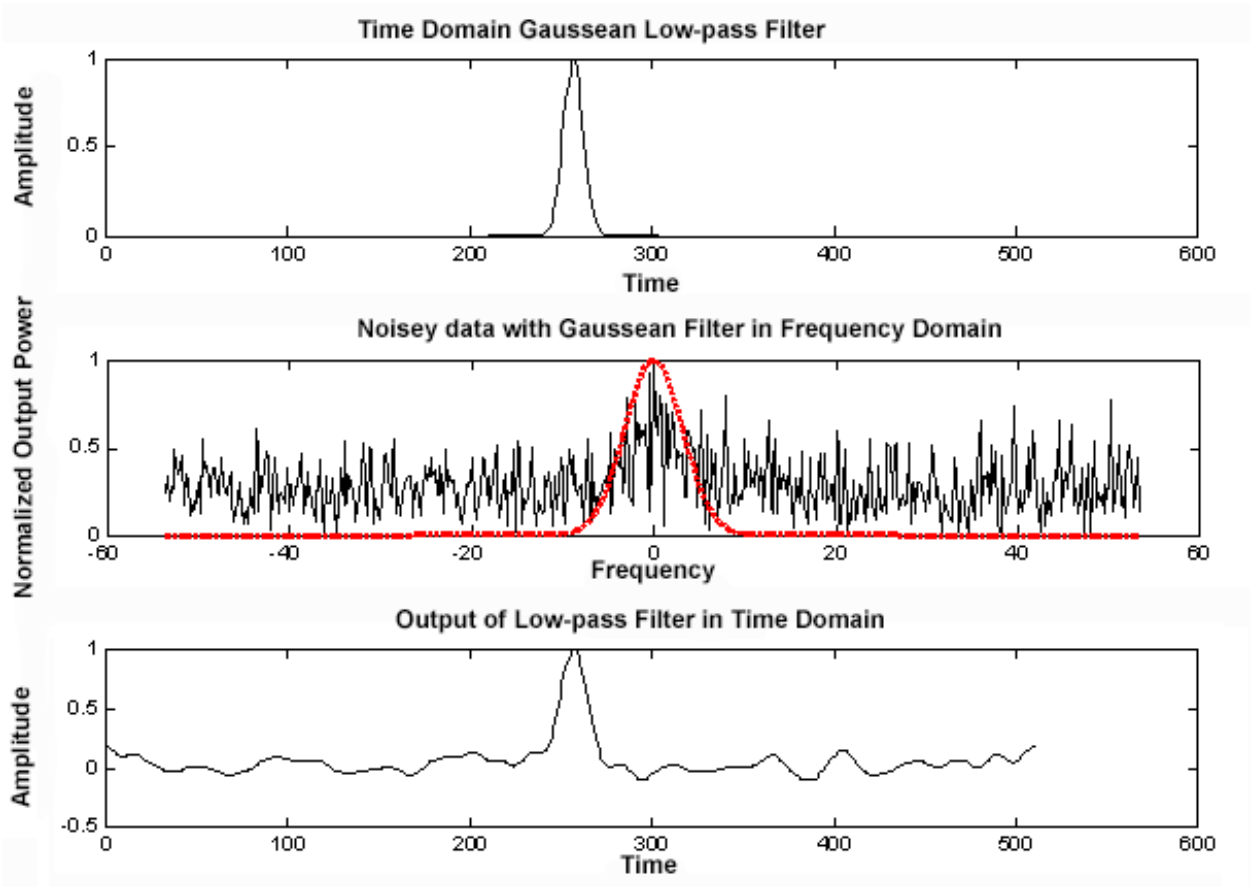

Figure 2. Processing of Noisy Data With Gaussian Low-Pass Filter

Lock-in Amplifiers

A much more effective approach for processing IR detector outputs is the lock-in amplifier. The lock-in approach works with the assumption that the output voltage from the IR detector is coherent with, and behaves in the same manner as, the reference (or loading) signal. That is, cyclic loading of a target specimen should cause a cyclic IR detector output. When this condition holds, a lock-in amplifier is capable of isolating rich thermoelastic information from heavily noisy output signals. The lock-in amplifier consists of amplifiers, a signal mixer and low-pass (or band-pass) filters. A block diagram of the lock-in amplifier is shown in Figure 3. The phase shifter adjusts the timing of the reference signal, forwards or backwards in time, until an optimal response is obtained. For more information on the phase shift contribution, refer to the corresponding pseudo-code in the Appendix.

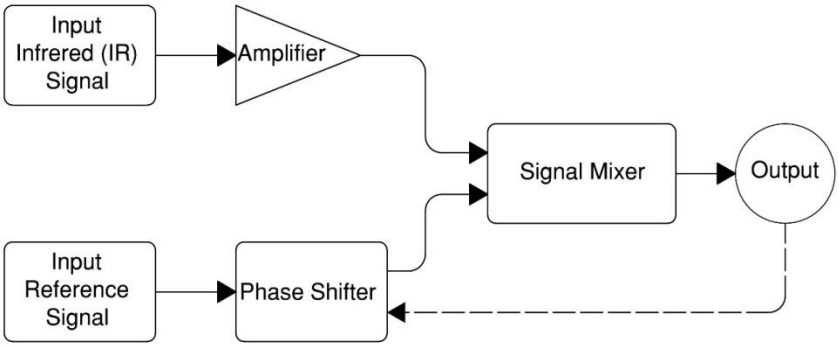

Figure 3. Block Diagram for a Lock-in Amplifier

Amplifiers

The amplifiers increase the amplitude of a small input IR signal. This increases the amplitude of both the thermoelastic signal and the noise in the input. Differential amplifiers could be used to reduce the amplification of noise in the output.

Mixers or Multipliers

The signal mixer is the heart of the lock-in amplifier. It is used to isolate part of the detector output that is synchronous with the loading (or reference) signal. This is achieved by correlating (or multiplying) the IR detector signals with the reference signal. In the time domain, mixing two signals is the same as taking a dot product of the two signals. The idea being that the product of two signals that are of like sign (positive or negative) is positive; whereas, the product of two signals with unlike signs is negative. In the frequency domain, mixing (by convolution) two signals of distinct frequencies f_1 and f_2 will yield a resulting output which has frequency content of $f_1 + f_2$ and $f_1 - f_2$. The IR detector output contains thermoelastic response and noise. Therefore, mixing the response frequency ($f_r + f_n$) with the reference frequency (f_r) will cause some of the output to be direct current (DC) signal or $[f_r - f_r]$ and the other portion to be twice the reference frequency $[2f_r]$. Contribution of the noise component in the DC output is negligible, and hence can be omitted.

Low-pass filter

After signal mixing, the resulting signal product is passed through a series of low-pass filters (e.g., averaging and Gaussian low-pass filters) to obtain the required thermoelastic response signal. In the time domain, a simple averaging of the correlated signal is enough to extract a useful thermoelastic signal. In the frequency domain, the thermoelastic signal corresponds to the DC component. To remove the DC component of the signal from the mixed output, a low-pass filter is needed to remove the portion of the signal which is above a pre-defined cut-off frequency.

A key challenge to the use of lock-in amplifiers is the need to acquire a reference signal; in practice, this may be difficult. Also, the thermoelastic response signal may be corrupted if the noise in the detector output is correlated with the reference signal.

Time-Frequency Domain Signal Processing

The current study adopts a time-frequency domain lock-in approach to process IR data. With this approach, the signal mixer is implemented in the frequency domain by way of a Fast Fourier Transformation (FFT), which converts the time-domain signals, of both the IR images and the reference signal, to frequency-domain signals. This provides a convenient way to measure the strength of the signal at a particular frequency, or the noise in the signal as a function of frequency. Using this functionality improves the effectiveness of the lock-in algorithm. The images resulting from the signal mixing process are then filtered in the frequency domain using a Gaussian filter. Subsequently, images are then filtered in the time domain using a time-averaging filter. The time-frequency domain lock-in (shown in Figure 4) is designed as follows:

- *Step 1:* Synchronize camera output with reference load signal using timestamps or phase information.

- *Step 2:* Take the Fourier transform of the IR images and the reference signal, where $x(t)$ and $y(t)$ correspond to the IR signal and the reference signal outputs, generated as a function of time, respectively. Thus, the FFT of $x(t)$ and $y(t)$ are of the form in Equations 8 and 9:

  $$F_x(\omega) = \int x(t)e^{-i\omega t}dt \qquad \text{Eq. 8}$$

  $$F_y(\omega) = \int y(t)e^{-i\omega t}dt \qquad \text{Eq. 9}$$

  The power or strength of the signal at different frequencies can be designated as in Equation 10:

  $$|F| = F_x(\omega)F_x^*(\omega) \qquad \text{Eq. 10}$$

  where the superscript (*) of Equation 10 denotes complex conjugate.

- *Step 3:* With the strength of the signal and noise known, low strength [noise] signals are removed using a low-pass and band-pass filter using Equation 11.

  $$F_{\bar{x}}(\omega) = F_x(\omega) \circ H(\omega) \quad \text{Eq. 11}$$

  where ∘ designates element-wise multiplication (Hamadard product) and
  $H(\omega) =$ *Filter at a certain function of frequency*

- *Step 4:* Correlate results in Step 3 with the Fourier transformed reference signal using Equation 12:

  $$X(\omega) = F_x(\omega) \circ H(\omega) \circ F_y(\omega) \quad \text{Eq. 12}$$

- *Step 5:* An inverse Fourier transform (IFFT) is performed on $X(\omega)$ to return the result back to the time domain.

  $$\bar{x}(t) = IFFT[X(\omega)] \quad \text{Eq. 13}$$

- *Step 6*: $\overline{\overline{x(t)}}$ is finally passed through a time averaging low-pass filter to remove random noise.

  $$\overline{\overline{x(t)}} = \sum_{\forall t} \bar{x}(t) \quad \text{Eq. 14}$$

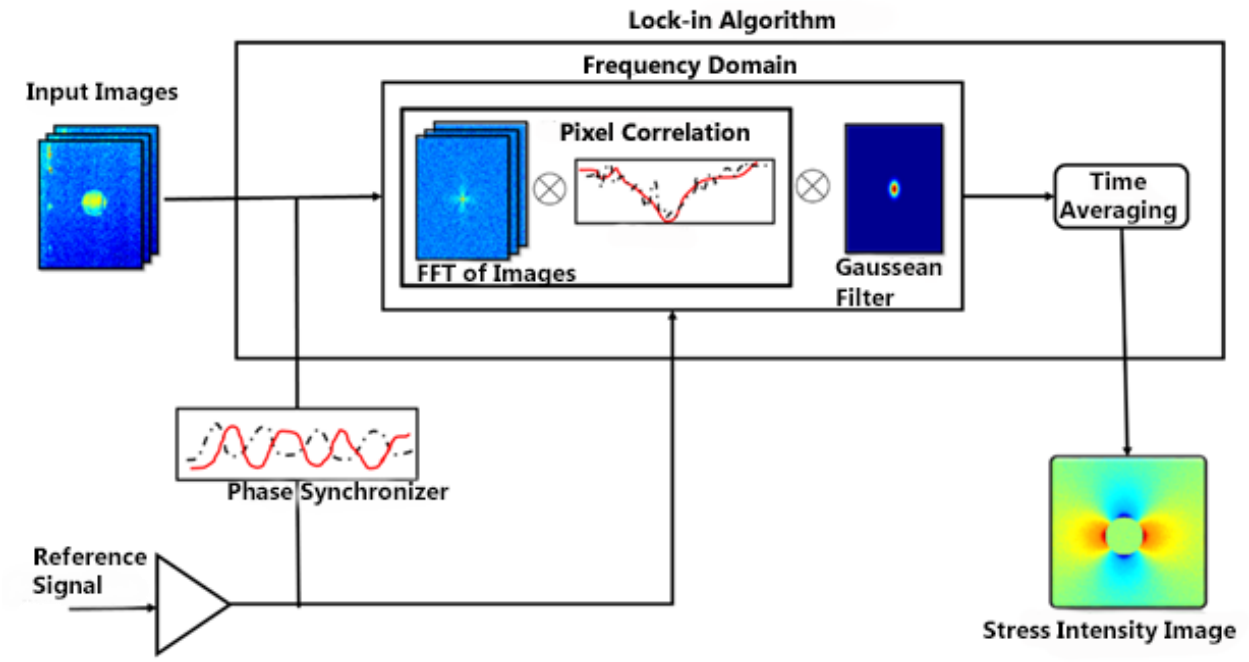

Figure 4. Time-Frequency Domain Data Processing

Proof of Concept

A successful proof of the TSA concept, using cyclical loading, was previously reported by Kantner (2012). The current work extended the TSA concept to the full-field stress analysis of steel structures, exposed to loading magnitudes and rates that typify those observed on bridges instead of using cyclical loading. Proof of this concept was demonstrated through computer simulations, laboratory experiments, field-testing and measurements.

Computer Simulation of Thermoelastic Responses

The key components for simulating the thermoelastic response of a specimen include:

- Reference Signal Simulations: a reference signal that simulates the loading events applied to the specimen over time.

- IR Data Capture Simulations: a simulated signal that reproduces expected IR camera response to surface temperature changes with simulated noise over time.

- Signal Processing: an algorithm for extracting thermoelastic information from simulated temperature changes.

Each of these aspects was addressed during computer simulations using finite element modeling software to simulate the mechanical and thermal response to simulated loading of a simple plate with a hole, loaded vertically in uniaxial tension resulting in plane stress. The modeling aided in development of a robust laboratory and field-ready method for extracting thermoelastic stress data from randomly loaded elements. The program simulated both the radiation heat transfer from a hole-in-plate model and the impact of varying levels of signal noise that would be encountered during IR data capture. The simulation was performed to confirm the theoretical stress values prior to laboratory testing.

Reference Signal Simulations

Previous TSA simulations, or experiments, assumed sinusoidal loading to characterize field events. However, sinusoidal loading assumes that the speed (frequency) and the stress level (amplitude) of each event are constant over time. In practice, these parameters usually change randomly. Figure 5 shows three different types of reference signals used in this work to validate the extended TSA concept. The first signal is a simple sinusoidal reference signal with constant amplitude and frequency. The second reference signal varies in amplitude but frequency stays the same. The third reference signal randomly changes in both amplitude and frequency.

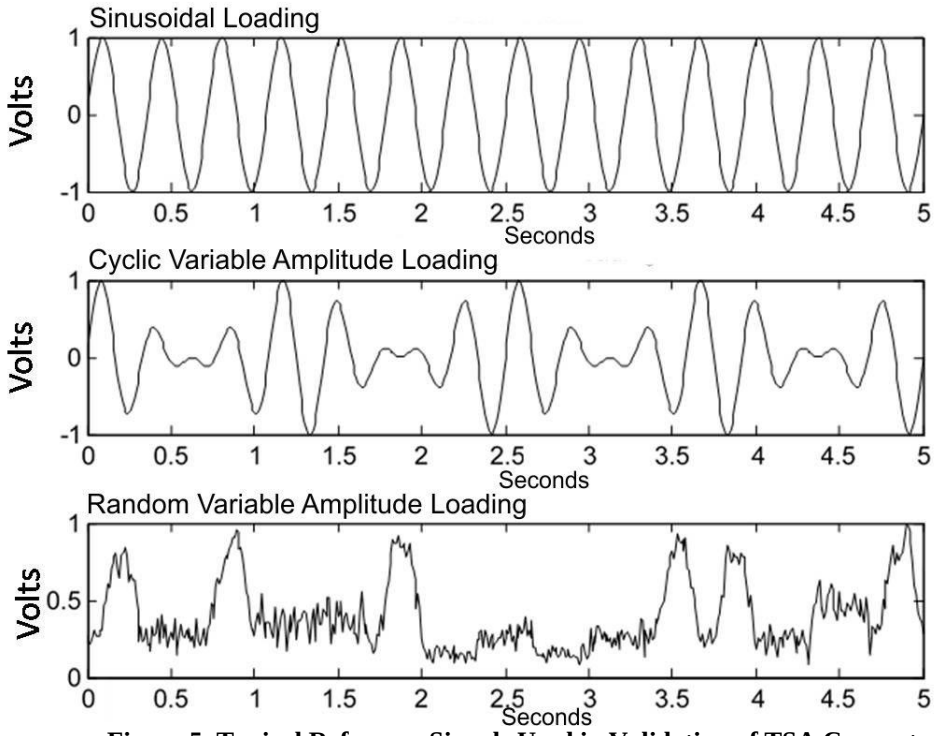

Figure 5. Typical Reference Signals Used in Validation of TSA Concept

Laboratory Testing

To confirm and extend the results of the computer simulations, thermoelastic stress analysis was performed on a prototype system in the laboratory. Laboratory experiments were also used to develop, define and refine the capabilities and limitations of the TSA system under controlled, yet realistic conditions. A steel specimen, under dynamic loading, was used in the replication of the sort of stresses and distortions associated with a typical bridge detail. The set up for performing TSA in the laboratory consisted of four key components:

1. a steel specimen
2. an uncooled microbolometer IR camera
3. an MTS loading frame
4. a custom-built computer unit.

Specimen

A steel specimen, shown in Figure 6, having a ½-in diameter hole drilled through its center was used in the laboratory experiments. The hole-in-plate specimen was 12 in long, 2 in wide and 1/8 in thick. The area around the hole was coated with a flat black paint, as explained in the theory section, due to the low and variable emissivity of hot-rolled steel. The yield strength of the specimen was unknown; however, during testing the specimens were exposed to stresses as high as 44 ksi, with no observable yielding.

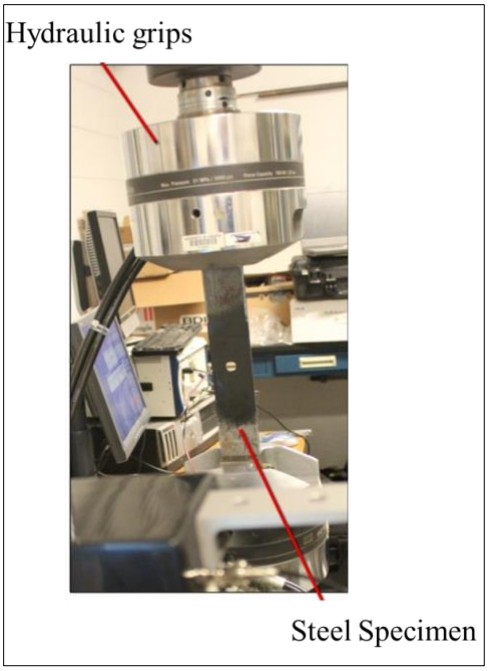

Figure 6. Hole-in-Plate Specimen Held in Place by Hydraulic Grips

Camera

An uncooled microbolometer camera, shown in Figure 7, was used for the laboratory experiments. The camera has a fixed focal length and was positioned approximately 2 feet from the specimen. The analog signal from the camera was transmitted to a monitor for real-time viewing. The digital output from the camera was fed into a custom-built computer, designed by Fuchs Consulting, Inc., which saved the image files. The digital images are 256 by 324 pixels and have 16-bit depth. The maximum frame rate of the camera was 60Hz.

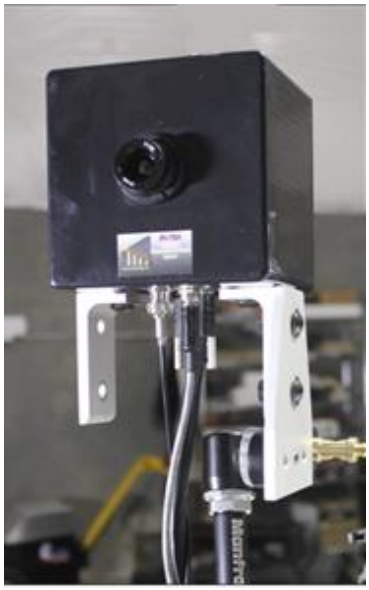

Figure 7. Microbolometer IR Camera

MTS System

The MTS system, a servo-hydraulic load frame system, was used to apply loads (force) to the steel specimen. The system includes a loading frame that holds the specimen, a hydraulic pump, an actuator to create the force and a computer with specialized software used to coordinate the actuator movement. The system can be programmed to apply loads that are similar to those expected in the field. The user-programmed time varying loads, generated by the frame, are also used as the reference signal for the lock-in process. The reference signal produced by the MTS loading frame is acquired directly by the custom-built computer, sampled at a rate of 1000 Hz.

Custom-Built IR-TSA System

The IR-TSA system, shown in Figure 8, contains an embedded computer, which is responsible for triggering data collection from both the IR camera and the embedded data acquisition system. Data collected with the embedded data acquisition system can include a high-level signal from the MTS system output or a low-level direct strain gage signal. The system is also able to be programmed to simultaneously acquire pre- and post-triggering data from the microbolometer IR imager and the reference signal over a user-defined duration. The IR camera data are saved as a video file. More specifically, the IR camera data are saved to an audio video interleave (AVI) file format, whereas the MTS output is displayed in volts. A schematic for how the different components function together is illustrated in Figure 9.

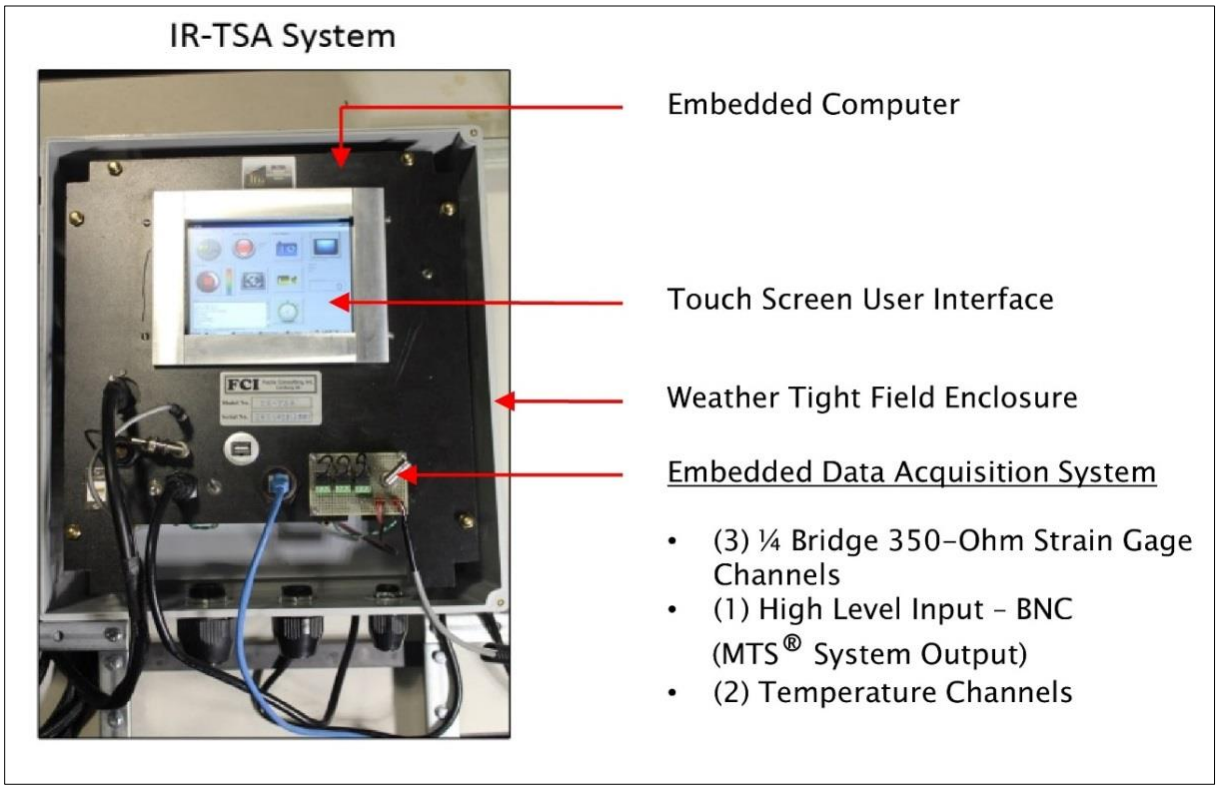

Figure 8. Custom-Built TSA System

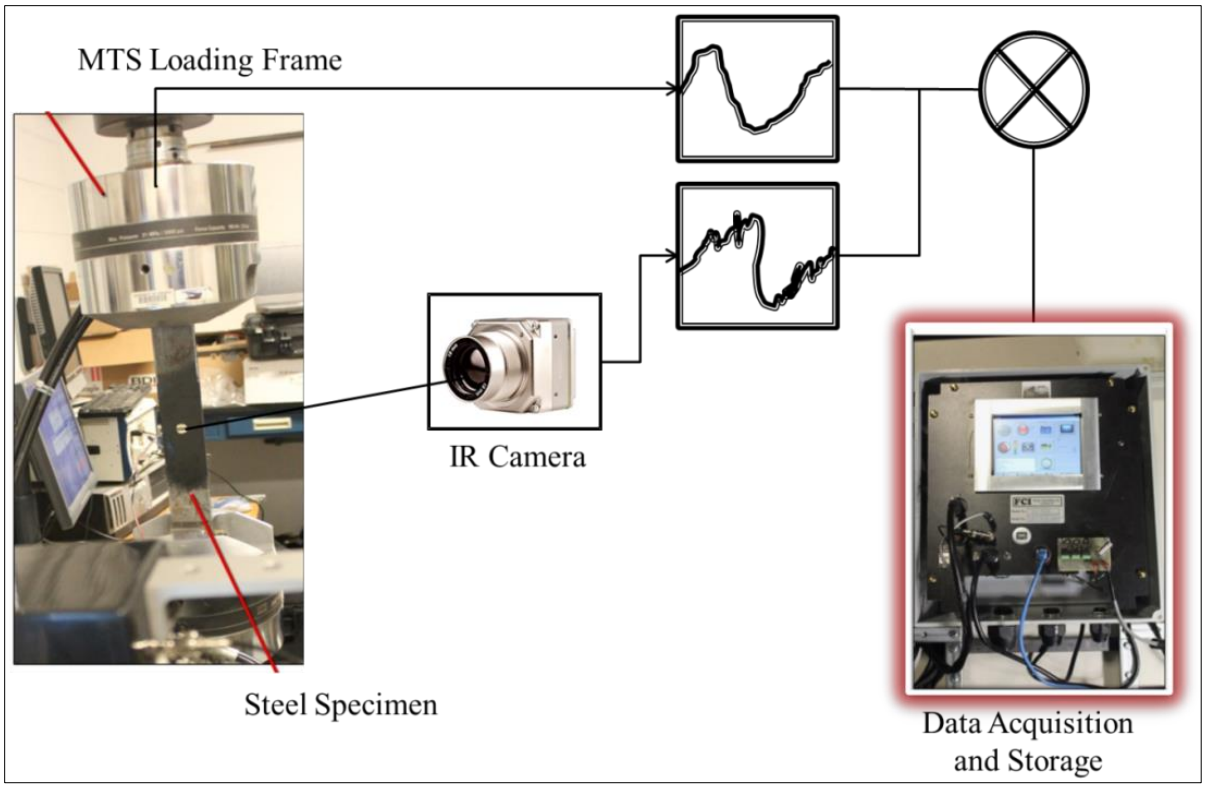

Figure 9. Key Components of Laboratory TSA System

Laboratory Testing Procedure

Once all the key components of the physical model were set up, testing began. First, a field-characteristic load program (or profile) was imported into the MTS systems computer software program. After all necessary parameters were set, the program was started and the defined loads were applied to the specimen.

Triggering and Data Acquisition

The system is designed to collect IR camera images (at high frame rates) and signals from the embedded data acquisition channels, simultaneously. Data are collected once the system detects a trigger event. Triggering may be configured in a number of ways, but is typically set as a simple [voltage] threshold for most data collection scenarios. A user-specified amount (seconds) of pre-trigger and post-trigger data is collected, stored, and processed for each triggered event. The system may be configured to trigger multiple times, with multiple corresponding data set collections. Trigger configurations may include a user-specified number of events, or as a time duration, over which an undetermined number of triggered events may be collected.

Data Acquisition and Display

Data acquisition begins once a triggering event is detected. Data acquisition includes the capture of both the pre-trigger and post-trigger data, as illustrated in Figure 10. The durations of

the pre-trigger and post-trigger data collection do not have to be equal. For example, if the total duration of data acquisition is to be 4 seconds, then duration of pre-trigger data would be set to 1 second and the duration of post-trigger data would be set to 3 seconds. Images from the IR camera are initially saved as AVI files, which are later converted into frame-by-frame multipurpose internet mail (MIM) files for post processing in MATLAB. Due to differences between the sampling rates of the IR camera and the MTS systems output, final data synchronization is carried out to match each IR image to with a corresponding reference load.

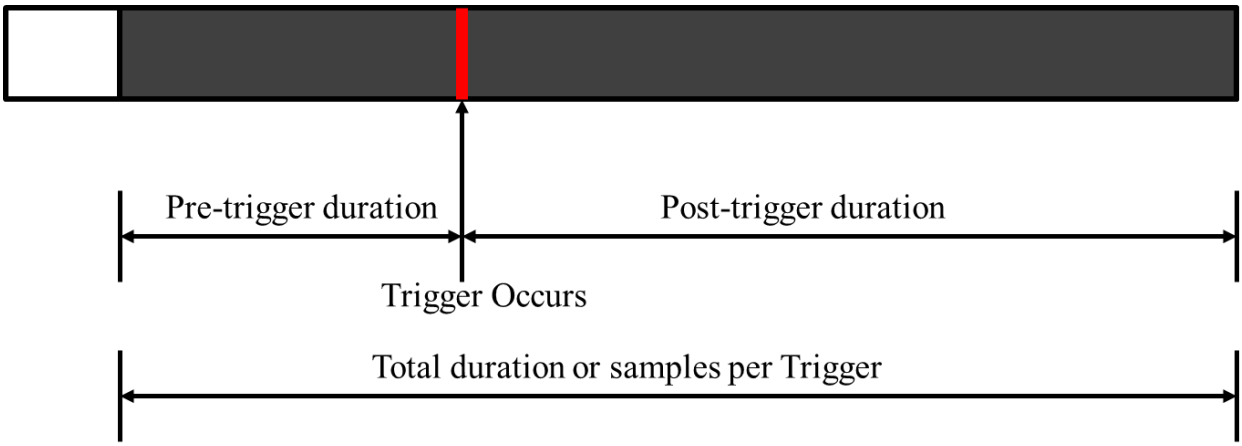

Figure 10. Capturing Pre- and Post-Trigger Data

Field Testing and Evaluation

After the successful laboratory testing, the TSA system was tested under actual field conditions. The IR-TSA system was deployed on an in service steel bridge, shown in Figure 11. The system was installed and set up to collect IR response data, when triggered by random vehicular events over time. The delta-frame bridge, selected for field evaluation of the IR-TSA system, is located along Interstate 64, in Rockbridge County, Virginia. This bridge was built in 1976 and under normal operation, carries westbound traffic into the Lexington, Virginia, region. The bridge is 845 feet long and 43 feet wide with a roadway width of 39 feet.

The TSA system was deployed to measure full field stress at a detail where fatigue cracks have been a problem. The specific location tested was a floor beam to girder connection at the interior of the fascia girder on the south side of the Eastbound Bridge. The field deployment of the TSA system is shown in Figure 12.

The four components of the system; IR Camera, Field Computer, Trigger sensor and power supply are shown. The installation of the TSA system was challenging, as it required the use of an under-bridge snooper to access the desired detail.

Figure 11. Delta-Frame Bridge Over Maury River on Interstate 64

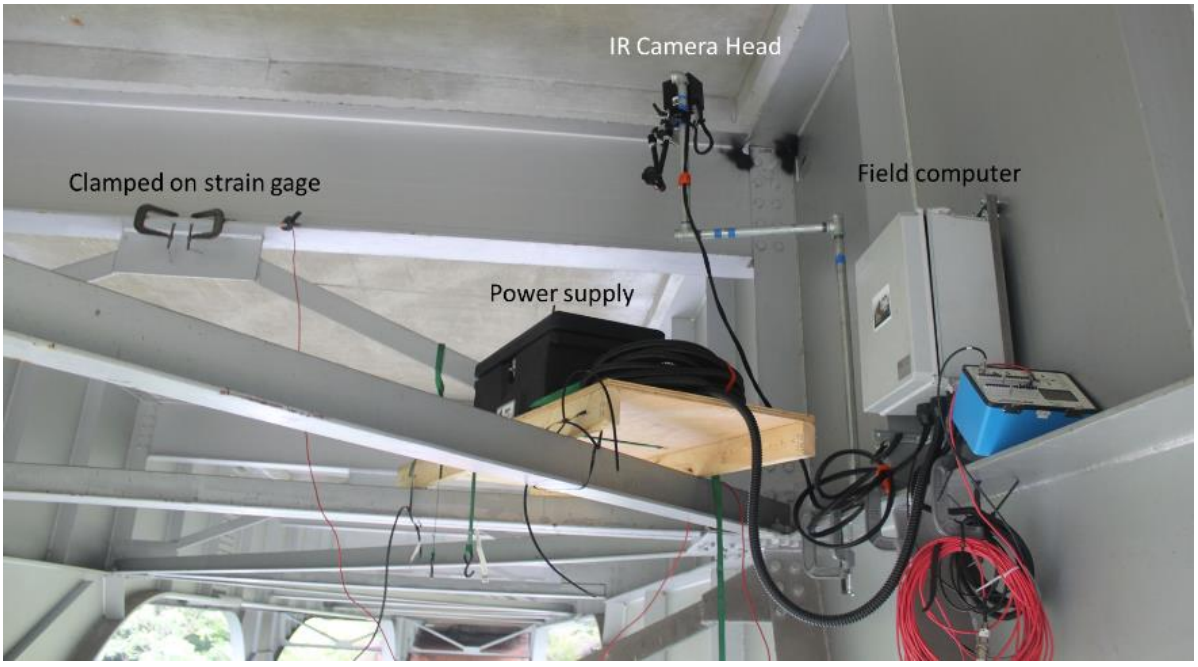

Figure 12. Field Deployment of IR-TSA System (Left) and IR Camera Viewing a Fatigue-Prone Detail (Right)

RESULTS

The results obtained during the laboratory and field testing described in the Methods section are reported here.

Parametric Model and Simulation

Computer simulation was performed to help understand the challenges and formulate solutions to use of reference signals, IR data capture, and signal processing before implementation in hardware. The results also aided in formulating subsequent testing plans.

Consider the plate shown in Figure 13a, which is loaded in tension to a nominal stress (σ). Assume the outer dimensions of the plate are infinite when compared to the diameter of the hole. From elasticity theory (Timoshenko and Goodier, 1951), the overall stress distributions around the central hole in the plate are given in polar coordinates by Equations 15 through 17:

$$\sigma_r = \frac{1}{2}\sigma\left(1 - \frac{a^2}{r^2}\right) + \frac{1}{2}\sigma\left(1 - \frac{4a^2}{r^2} + \frac{3a^4}{r^4}\right)\cos(2\theta) \quad \text{Eq. 15}$$

$$\sigma_\theta = \frac{1}{2}\sigma\left(1 + \frac{a^2}{r^2}\right) - \frac{1}{2}\sigma\left(1 + \frac{3a^4}{r^4}\right)\cos(2\theta) \quad \text{Eq. 16}$$

$$\tau_{r\theta} = -\frac{1}{2}\sigma\left(1 + \frac{2a^2}{r^2} - \frac{3a^4}{r^4}\right)\sin(2\theta) \quad \text{Eq. 17}$$

From Equations 15 through 17, we can determine the stresses on the edge of the hole by setting the radial distance variable equal to the radius of the hole ($r = a$). Stresses in the radial direction and shear stresses will be zero, while stresses in the angular direction will be given by $\sigma_\theta = \sigma(1 - 2\cos(2\theta))$. This will yield a maximum value of 3σ when $\theta = \pi/2$. Of course, everything is symmetric about the horizontal axis, so the stress is also 3σ at 3π/2. This is the maximum stress value anywhere around the circle. The ratio of this stress value to the nominal stress value is defined as the maximum stress concentration factor K_{tg}. This stress concentration factor scales the nominal stress, which exists far away from the hole (i.e. σ). This factor is meant to take the loss of cross-sectional area into account; however, since the plate in Figure 13a is infinitely wide, the loss of cross-sectional area is irrelevant. Consequently, it is appropriate to use a related stress concentration factor, K_{tn}, that does take the loss of section into account. The related concentration factor, K_{tn}, is given by Equation 18, where d is the diameter of the hole and H is the width of the plate. When a finite width is considered (as shown in Figure 13b) it has an effect on the stress concentration factor. With the geometry of the test specimen used, the adjusted stress concentration factor will be about 3.23 σ.

$$K_{tn} = \frac{2 + \left(1 - \frac{d}{H}\right)^3}{1 - \frac{d}{H}} \quad \text{Eq. 18}$$

The simulation response shown in Figure 14 was generated with a program created in MATLAB based upon the above equations. The program simulated both the radiation heat transfer from a hole-in-plate model and IR data capture. Figure 14 shows the calculated thermoelastic response for a thin plate subjected to uniaxial tension. The temperature change calculated is based on the sum of the principal stresses.

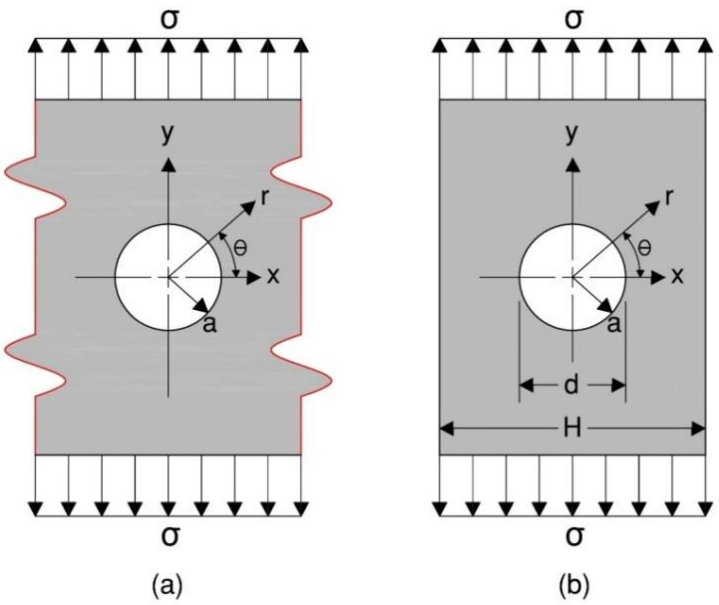

Figure 13. Diagram of a) infinitely Wide Plate With Hole and b) Plate of Finite Width With Hole, Each Loaded Vertically in Uniaxial Tension

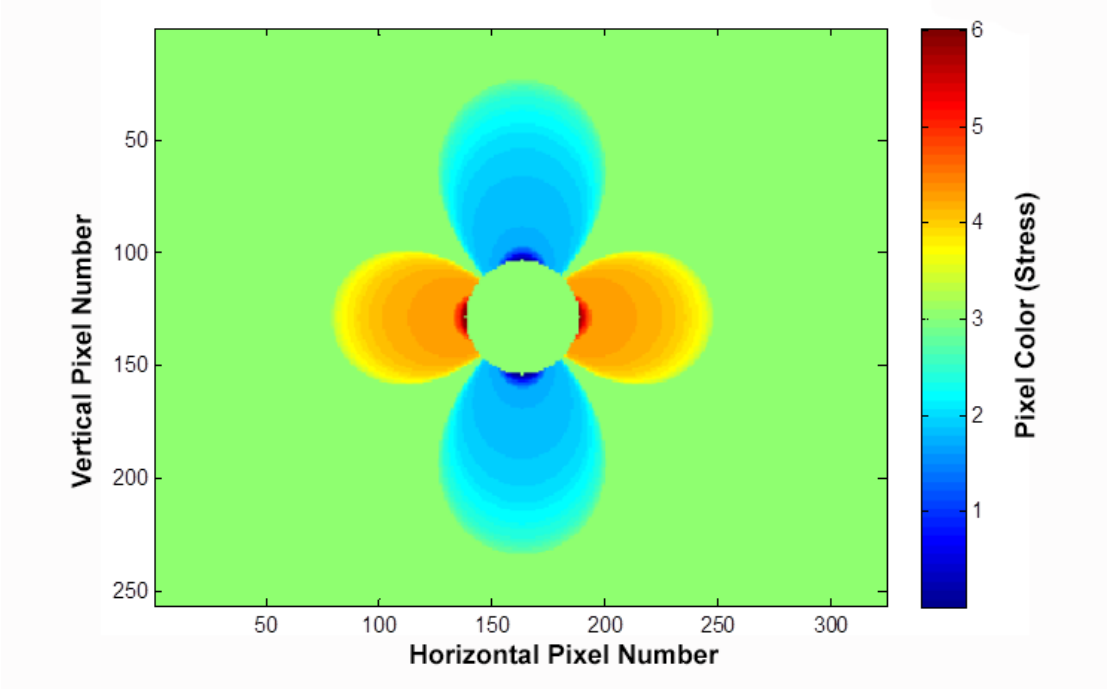

Figure 14. Simulation of Theoretical Stress Concentration for a Hole-in-Plate Specimen

IR Data Capture Simulations

The stress levels applied in the laboratory produced temperature changes that are barely detectable even with highly sensitive photonic IR cameras. The simulations described in this section created images that are representative of what can be attained with a microbolometer camera for varying stress levels. The output temperature is based on the theoretical temperature change for the corresponding stress variation. The output temperature was converted to an unsigned 16-bit integer format (just as the camera would produce). Random numbers, sampled from a uniform distribution, were generated using the MATLAB random number generator and used to add noise to the output image. This simulated both the electronic and environmental noise that contaminates the microbolometer camera output. The interval over which the noise is sampled may be varied depending on the level of corruption desired.

Corruption Levels

The calculated level of image corruption is based on the peak signal-to-noise ratio (PSNR) of the image. PSNR is the ratio between the maximum power of an image and the power of the corrupting noise and is defined via Mean Squared Error (MSE) as in Equations 19 and 20:

$$PSNR = 10 * log_{10}\left[\frac{\max\{s^2(i,j)\}}{MSE}\right] \quad \text{Eq. 19}$$

$$MSE = \frac{1}{M*N}\sum_{i=0}^{M-1}\sum_{j=0}^{N-1}[x(i,j) - s(i,j)]^2 \quad \text{Eq. 20}$$

where

$M, N = Number\ of\ pixels\ in\ horizontal\ and\ vertical\ directions$
$i, j = Indices$
$s(i,j) = Value\ of\ pixel\ in\ uncorrupted\ image$
$x(i,j) = Value\ of\ pixel\ in\ corrupted\ image.$

Figure 15 shows results from three sets of simulations, with varying levels of corruption, resulting from a purely sinusoidal reference signal at a frequency of 3 Hz. As illustrated by the cross-sectional pixel intensity profiles (or profiles) in the figure, the thermoelastic signal is imperceptibly buried in noise at a corruption level (or PSNR) of -2. The next section explains steps for extracting useful thermoelastic information from the corrupted images.

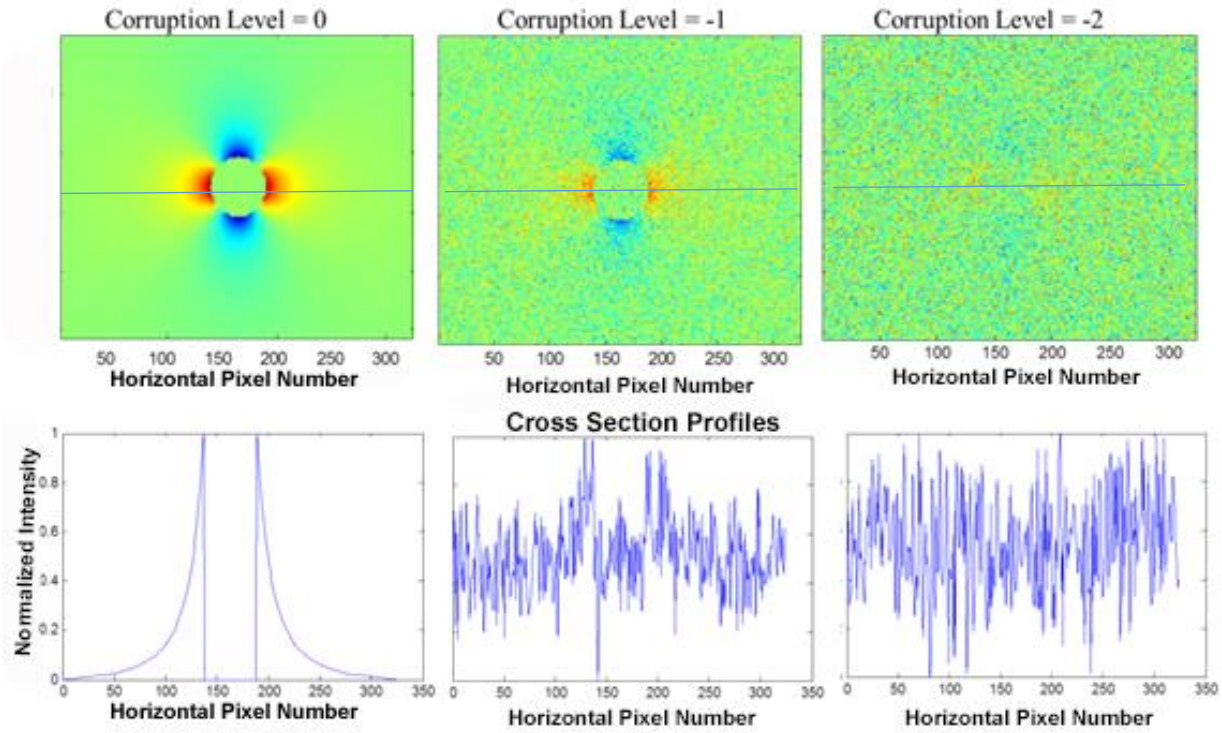

Figure 15. Simulation of IR Data Capture for Different Levels of Corruption

Signal Processing

As observed in Figure 15, the thermoelastic signal is not visible in the image produced by the microbolometer camera; the signal is completely buried in noise. Lock-in thermography was used to extract the desired thermoelastic signal from the background noise. To evaluate the effectiveness and applicability of the lock-in signal-processing algorithm to real field data, the following experiments were conducted.

Robustness of Lock-in Algorithm Against Noise

The first experiment investigated the ability of the lock-in algorithm to extract thermoelastic signals from corrupted IR images. Figure 16a shows examples of simulated microbolometer images at their respective levels of corruption. It can be seen that the thermoelastic signal is completely obscured at a corruption level of -5. The thermoelastic response extracted at different levels of corruption using the lock-in algorithm is shown in Figure 16b. It is evident that although time and frequency domain lock-in thermography is sensitive to the level of corruption of the IR camera data, the algorithm can be used to extract relevant stress information from image series with high levels of noise.

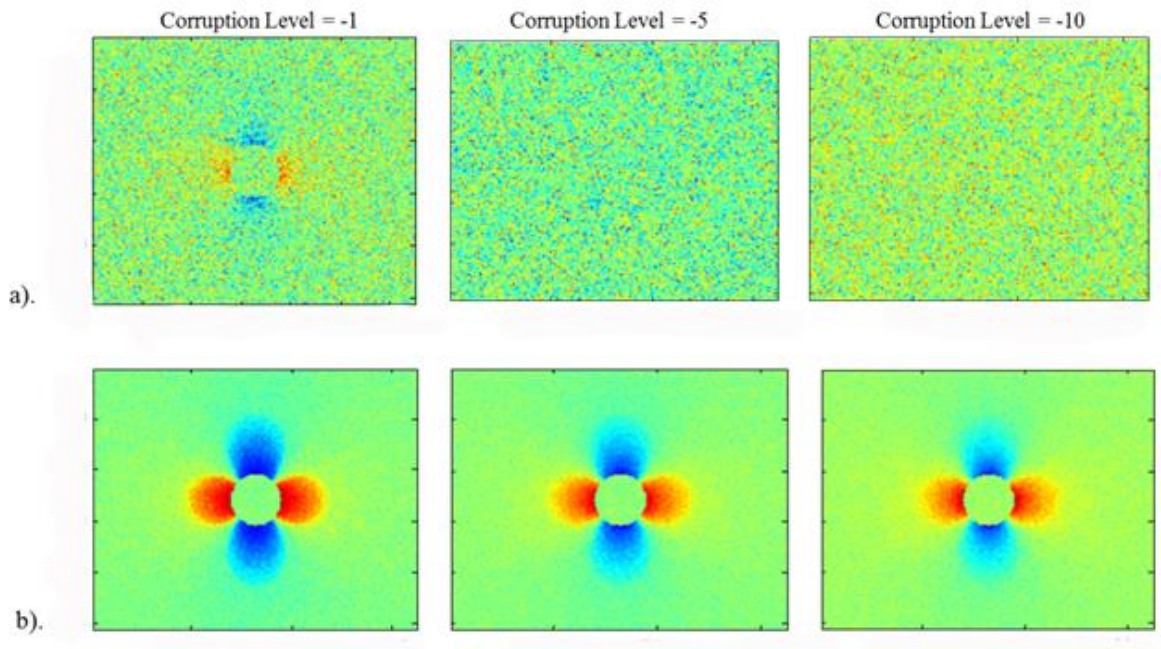

Figure 16. a) Simulated Thermal Images at Varying Levels of Corruption, and b) Extracted Thermoelastic Response Using Time and Frequency Based Lock-in Algorithm

Figure 17 shows a plot of level of corruption versus the signal to noise ratio SNR of the respective TSA images, extracted using variable amplitude and frequency loading rates. The SNR is calculated by comparing the thermoelastic signal extracted from a corrupted image to the signal extracted from a non-corrupted image; SNR is designated as:

$$SNR = 20 * \log\left[\frac{\|x\|}{\|x-y\|}\right] \quad \text{Eq. 21}$$

where

x = *Value of pixel in uncorrupted image*
y = *Value of pixel in corrupted image.*

The SNR value is computed for all pixels in the image and then averaged over the entire image.

By observation of Figure 17, time and frequency domain lock-in thermography could be used to extract TSA responses from images where the absolute value of the corruption level is less than 20; this is the practical maximum corruption level. Beyond this point, the thermoelastic response gets obscured and therefore cannot be used for any meaningful analysis or decision-making. It should be noted that for the traditional lock-in thermography algorithms the maximum corruption level was approximately 5.

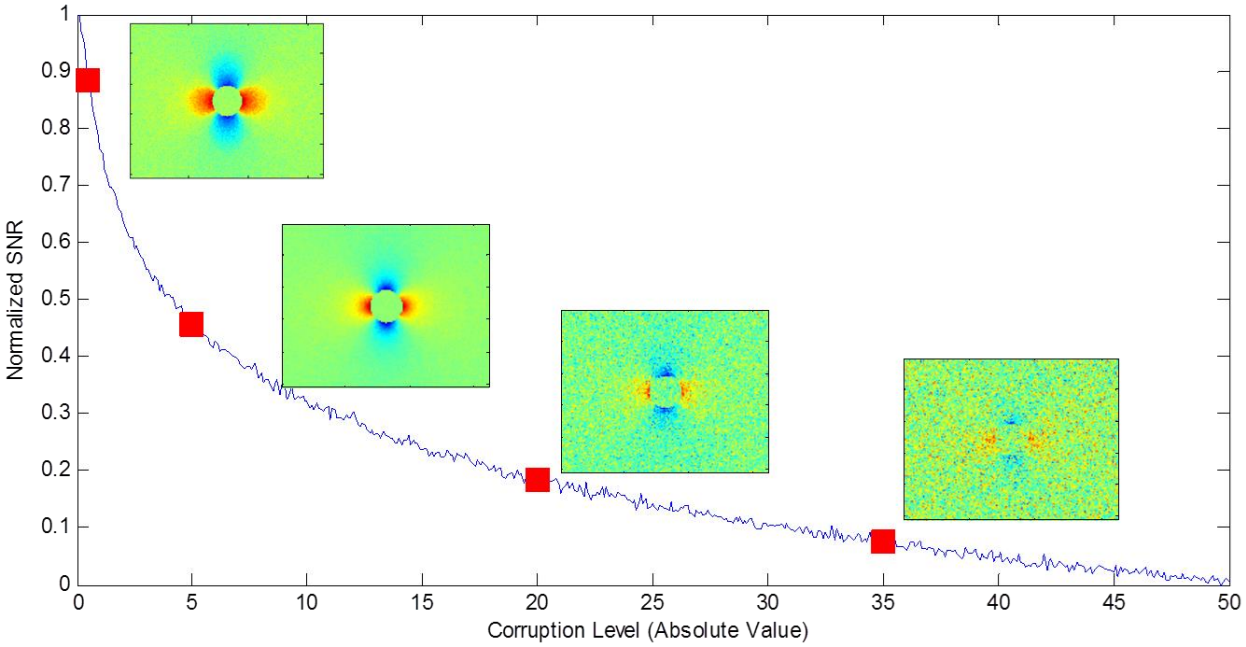

Figure 17. Illustrates Quality of Thermoelastic Response Extracted With Increasing Level of Corruption (Number of Events = 10)

The simulations demonstrated that the lock-in algorithm was capable of pulling a signal out of a very noisy environment, but applying this technology in the field or the lab has many more complications than does a simulation. The section on laboratory experiments with TSA discusses the further complications when the noise is due to actual phenomena, and not simply a random number generator.

Stress Levels and Minimum Event Data Recording Time

Field events of interest are mostly transient, random and occur over short periods of time. The TSA system is expected to capture useful information corresponding to such short-duration events. The following experiment explored the optimal length of time required to obtain a useful thermoelastic image from a series of transient events at varying stress levels.

Figure 18 shows thermoelastic response information extracted as a function of the total recording time per event (1, 2 and 3 seconds) for varying levels of tensile load (5 kip, 2.5 kip, and 1.25 kip). The modeled test specimen is similar to that shown in Figure 13b, having a width of 2 in, a thickness of 1/8 in, and a centered hole of 1/2-in diameter. The modeled load is uniaxial, in the vertical direction. The responses are based on a constant IR camera data collection rate of 60 Hz. By observing the responses provided in Figure 18, it is clear that the quality of response increases with increasing stress levels and total recording time.

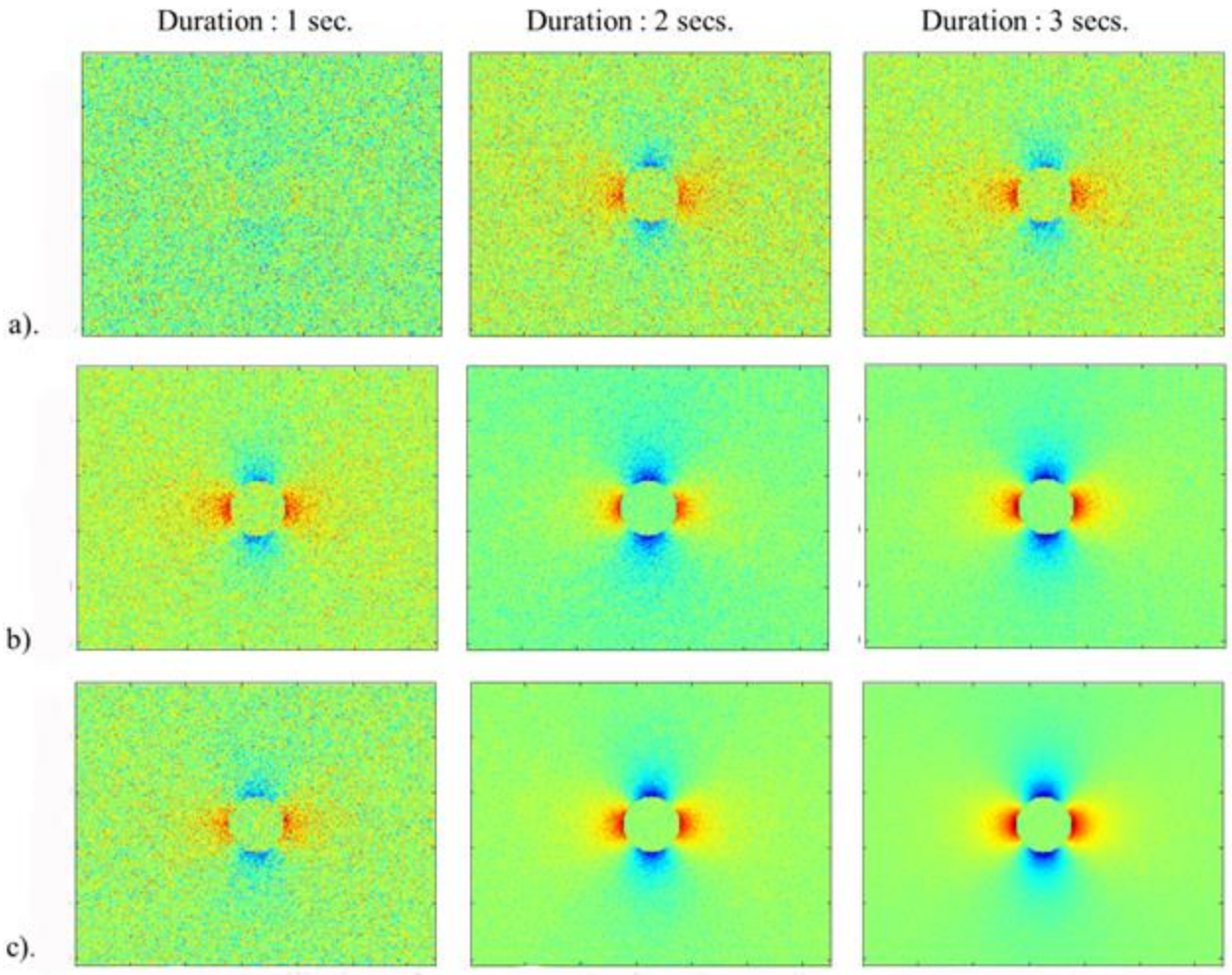

Figure 18. Simulated TSA Response Using Random Signal With Maximum Loading of a) 1.25 kip, b) 2.5 kip, and c) 5 kip

To identify the optimal recording length and stress level at which the lock-in algorithm produces a high-contrast image, the simulated response is compared with a corresponding theoretical response. The range of recording times per event is varied between 0.2 and 3 seconds. Each recording time consisted of a total of 10 events. That is, if the recording time is 0.5 second, then the frequency of events is 20 Hz. The TSA responses generated are from a purely random reference signal with maximum loadings of 5 kip, 2.5 kip, and 1.25 kip. Figure 19 shows the quality of the thermoelastic response information extracted as a function of total recording time and stress level. The metric used to quantify the quality of the simulated response is determined by calculating the contrast gradient difference between the simulated and theoretical responses.

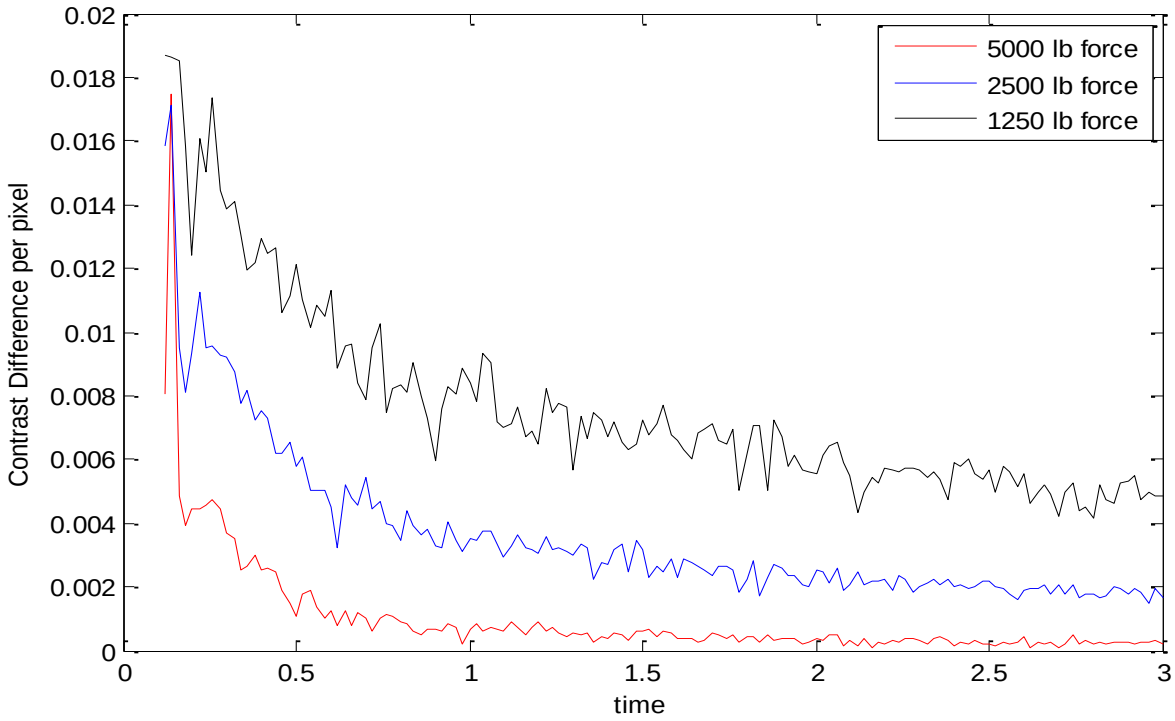

Figure 19. Reference Signal Consisted of Total of 10 Events per Second

From the results show in Figure 19, the simulated response approximately converges to the theoretical response after about 0.5 seconds for a reference signal with maximum force of 5,000 lb (5 kip), corresponding to a nominal stress of $\sigma = 20\ ksi$. Evidently, when the maximum force is less than 2,500 lb (2.5 kip), corresponding to a nominal stress of $\sigma = 10\ ksi$, the simulated response does not converge within 3 seconds. However, meaningful responses can still be extracted when the contrast difference per pixel is not more than 0.004. Therefore, an event with a maximum force of 2,500 lb., corresponding to a nominal stress of $\sigma = 10\ ksi$, with duration of 1 second, or more, will produce a thermoelastic response that may be resolved by the lock-in algorithm. Finally, based on Figure 19, an event with 1,250 lb. (1.25 kip), corresponding to a nominal stress of $\sigma = 5\ ksi$, will not yield a useful response for event durations of less than approximately 3 seconds.

Laboratory Experiments

The quality of the thermoelastic response extracted from the surface of a specimen subjected to dynamic loads is dependent on a number of factors, such as the number of events, stress levels (amplitude), traffic speed (frequency), camera view angle, emissivity of the specimen, etc. The following experiments were conducted to determine the capabilities and limitations of the IR-TSA system in terms of the aforementioned factors, under laboratory conditions intended to replicate conditions expected in the field. The data presented are based upon actual measurements taken using the IR-TSA system (i.e., not simulated).

An example of an output from the microbolometer IR camera is shown in Figure 20. The IR image shown contains a thermoelastic response buried in a large bandwidth of noise. The time and frequency domain lock-in algorithm can be used to extract rich thermoelastic

information from the noisy IR data as shown in Figure 21. To increase processing speed and resolution of the thermoelastic signal, a cropped area around the hole is supplied to the lock-in algorithm for processing.

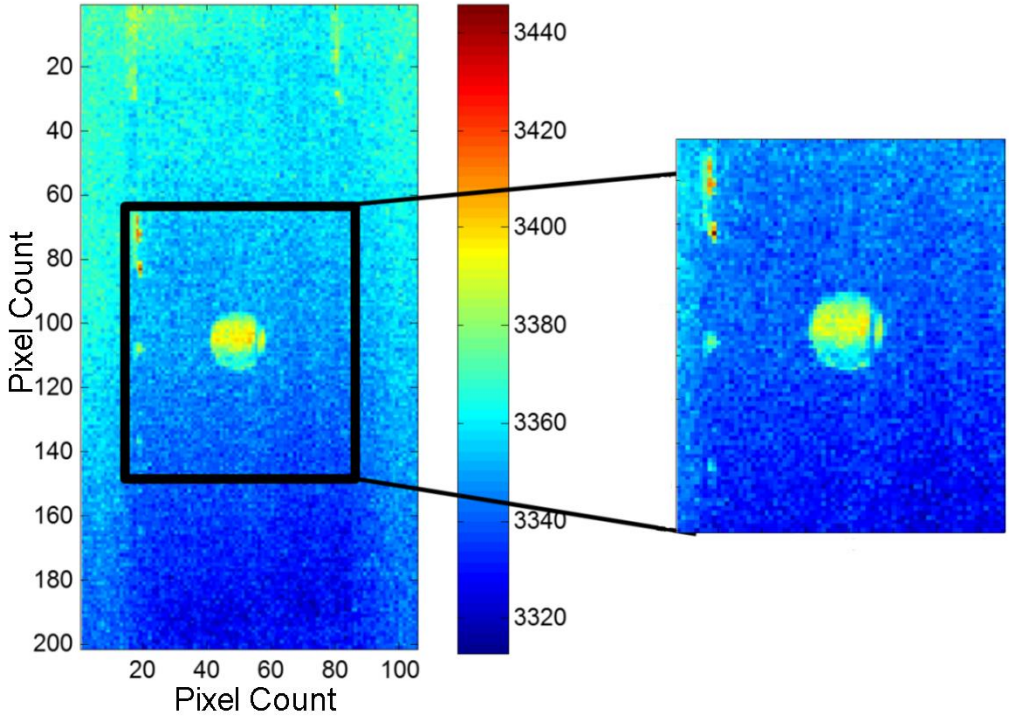

Figure 20. Sample Image Data (Un-Cropped and Cropped) Collected From Tau Microbolometer IR Camera

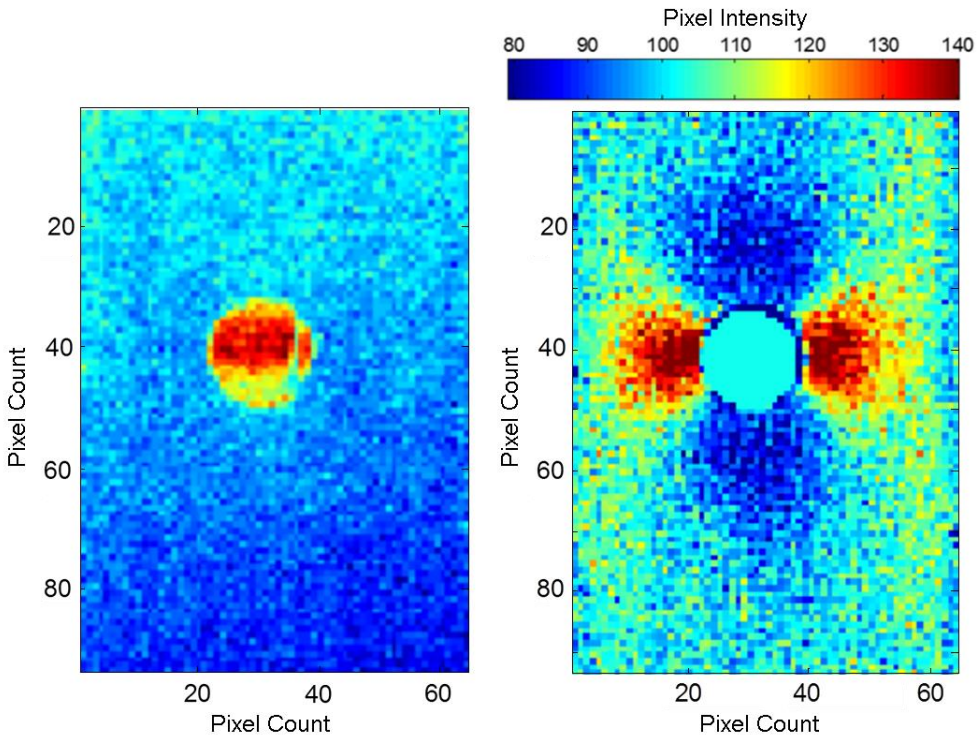

Figure 21. Raw Image and Processed Image Using Time-and-Frequency Domain Lock-in Algorithm

Loading Frequency and Amplitude Requirements and Limitations

It is expected that the amplitude, frequency and total duration of real field loading events will be generally random, due to random vehicle characteristics, loads and travel speeds on a bridge. The loading events generated in the laboratory by the MTS loading frame were designed to reproduce the inherent randomness in loading amplitude and duration of field events.

To evaluate the sensitivity of the IR-TSA system to loading frequency and amplitude, the field events were classified into three categories. The categories are based on the stress levels expected to be produced from various vehicular types. The categories include: low stress events (cars), medium stress events (light-duty trucks) and high stress events (heavy-duty trucks). Event classification attributes are summarized in Table 1. Although the IR-TSA system is designed to measure thermoelastic response from high-stress events, testing the systems response to low and medium stress events is also helpful for testing the limits of the technology. Two experiments were conducted to investigate the loading frequency and amplitude requirements and limitations.

Table 1. Loading Event Classification

Event Classification	Load (kip)	Nominal Stress (ksi)	Loading Duration per Event (sec)
Low Stress Events	0.5 – 1.25	2 – 5	0.5 – 2.5
Medium Stress Events	0.5 – 2.5	2 – 10	1.0 – 3.0
High Stress Events	0.5 – 3.5	2 – 14	1.0 – 3.0

Experiment 1

The first experiment focused on the extraction and evaluation of thermoelastic responses for each event classification in Table 1, at different travel speeds or frequencies. Figures 22 and 23 present the extracted TSA responses of each event classification, for both fast and slow moving vehicles, with loading durations of 2 and 3.5 seconds, respectively. From Figure 22a and b, it is evident that for events of at least 2 seconds duration, a useful thermoelastic response image is able to be extracted, when the maximum applied load is greater than or equal to 2.5 kip, corresponding to a nominal stress of 10 ksi. However, Figure 22c and Figure 23c indicate that the TSA technology is not useful for extracting stress levels with maximum loadings that are equal to or less than 1.25 kip, corresponding to a nominal stress of 5 ksi.

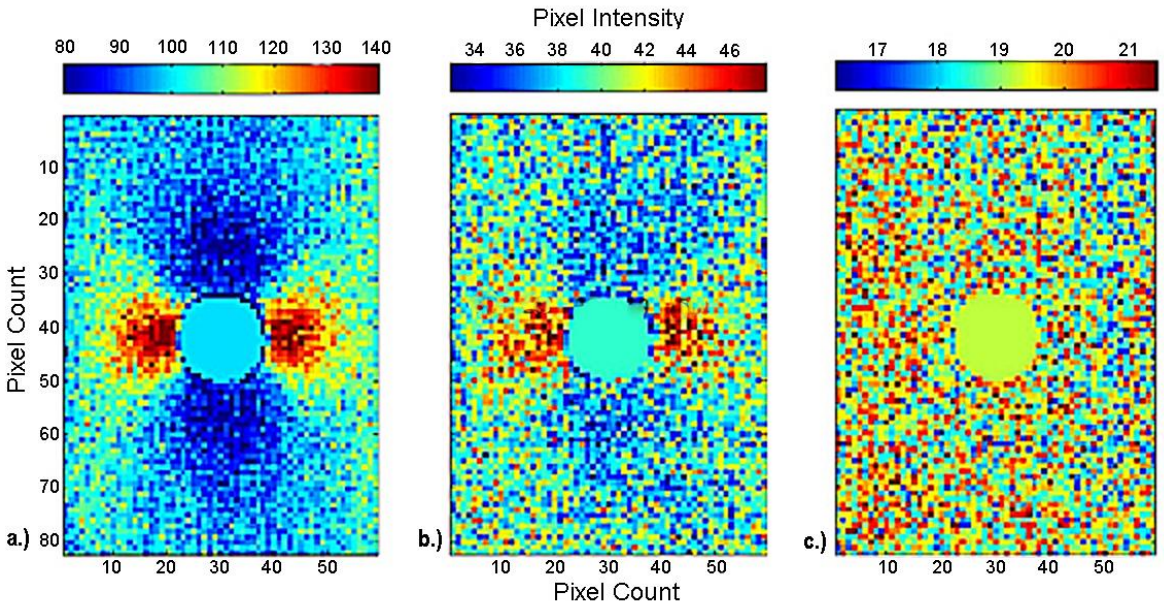

Figure 22. Characteristic Stress Concentrations Extracted for Different Stress Levels, Maximum Duration per Event = 2 Seconds, Total Number of Events = 20: a) 14-ksi Nominal Stress, 3.5-kip Max Load; b) 10-ksi Nominal Stress, 2.5-kip Max Load; c) 5-ksi Nominal Stress, 1.25-kip Max Load

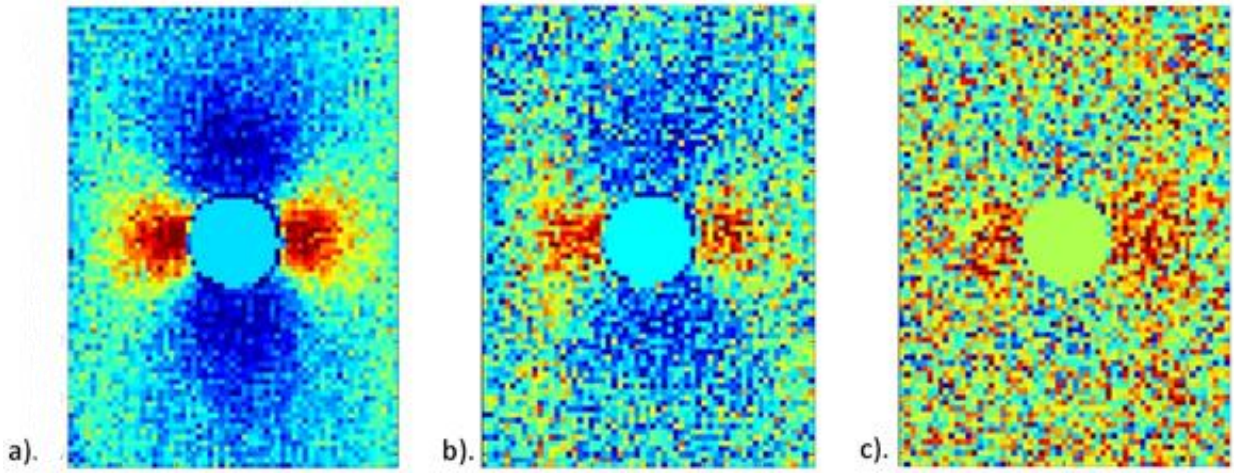

Figure 23. Characteristic Stress Concentration Patterns Extracted for Different Stress Levels (Maximum Duration per Event = 3.5 Seconds, Total Number of Events = 20): a) 14-ksi Nominal Stress, 3.5-kip Max; b) 10-ksi Nominal Stress, 2.5-kip Max Load; c) 5-ksi Nominal Stress, 1.25-kip Max Load

Experiment 2

In the second experiment, for the reference signal shown in Figure 24, the thermal response (shown in Figure 25a) is extracted from a specimen. The reference signal contains loading events from a mixture of all the event classification categories (i.e., trucks, light trucks and cars). The results show that although a useful thermoelastic response is obtained, the image quality is degraded. This is due to the inclusion of responses from high-speed cars, which generate negligible responses. Figure 25b shows that by removing the thermoelastic responses from low-stress events (i.e., cars) the contrast of the TSA images extracted are greatly improved.

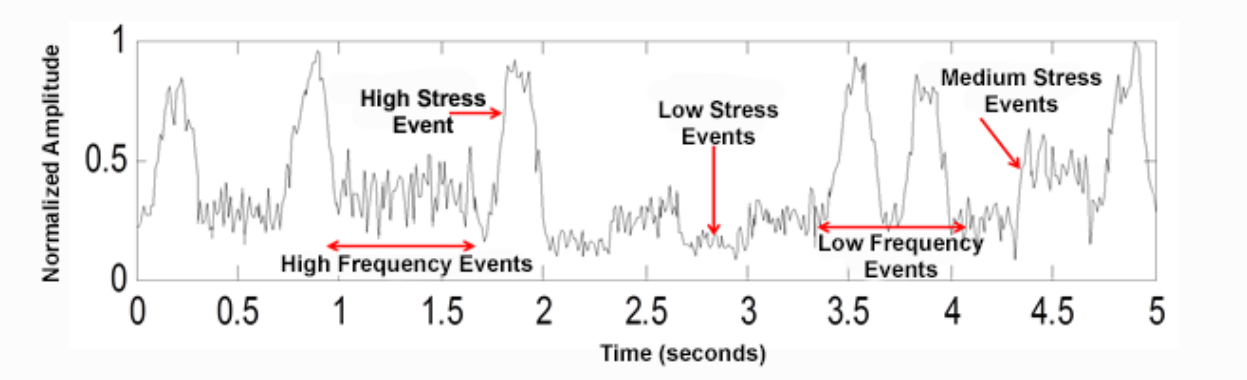

Figure 24. Input Reference Signal

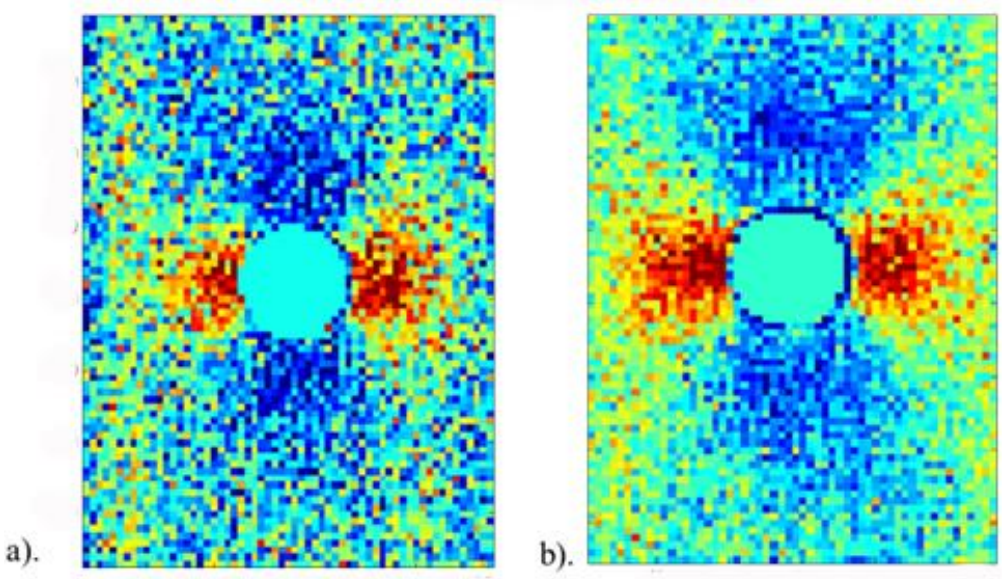

Figure 25. a) Thermoelastic Response for All Vehicle Types; b) Thermoelastic Response for Light and Heavy Trucks Only (No Cars)

Based on these results, it was concluded that the TSA system should be used to capture only those responses originating from high-stress events. This confirms the need to use a level triggered data acquisition approach.

Surface Preparation Requirements and Limitations

It is common for steel bridge structures to be protected by multiple layers of coating, which may be on the order of about 0.012 inches thickness (Mandeno and Sarraf, 2014). The coating system often consists of a prime coat, an intermediate coat and a finish or topcoat. The finish coat may be gray, green or brown in color. The typical range of coating layer thickness is provided in Table 2. It has been postulated that coatings could act as an insulating layer and thereby degrade the thermoelastic response or cause the detector signal to lag the loading frequency (Harwood and Cummings, 1991; Greenee et al., 2008). The experiment described in this section investigated this and resulted in recommended surface preparations necessary for effective field application of the IR-TSA technology.

Table 2. Coating Layers and Their Thickness (Myers and Washer, 2010)

Coating	Thickness (in)
Prime Coat	0.003 – 0.006
Intermediate Coat	0.003 – 0.005
Finish Coat	0.002 – 0.004

Experiment 3

The experiment was conducted in four stages, and the results are shown in Figure 26:

- *Stage 1:* Apply a gray finish coat (0.012 in. thick) to the steel test specimen and extract the thermal response.

- *Stage 2:* Apply a thin layer of black paint (0.008 in. thick) over the gray finish coat, from Stage 1, and then extract the corresponding thermal response.

- *Stage 3:* Apply another layer of gray finish coat (0.004 in. thick) over the black paint, from Stage 2, and then extract the corresponding thermal response.

- *Stage 4:* Finally, apply another layer of black paint (0.004 in. thick) over the gray paint, from Stage 3, and then extract the corresponding thermal response. It should be noted that at this final stage the total coating thickness is approximately 0.028 in.

Figure 26 shows that an application of flat black paint is necessary to extract useful thermoelastic response information. The flat black paint provides a uniform and highly emissive surface. The same figure shows that it is not necessary to remove existing paint before application of a black paint layer if the initial paint coating thickness is less than 0.03 inches.

During the laboratory experiments described so far, the IR camera was oriented at an angle perpendicular to the specimen. However, attaining a perpendicular orientation to fatigue-prone details in the field may be challenging or impossible. Consequently, in the field, the camera's view angle may become skewed.

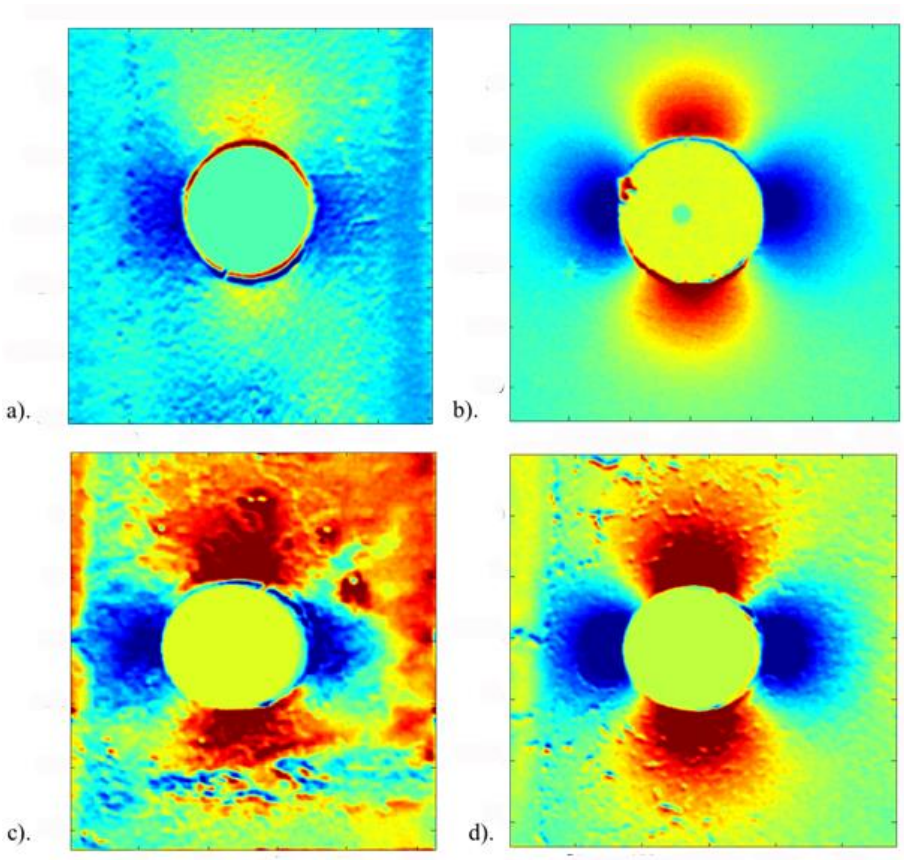

Figure 26. TSA Response to Different Paint Thickness: a) Flat Gray Paint 0.013 in Thick; b) Flat Black Paint Over Gray Paint 0.020 in Thick; c) Gray Paint Over Layers of Gray and Black Paint, Total Thickness 0.025 in; d) Black Paint Over 2 Layers of Gray Paint and a Layer of Black Paint, Total Thickness is 0.029 in.

Camera View Angle Requirements and Limitations

Experiment 5

The experiments described in this section investigated camera view angle requirements and limitations for the IR-TSA technology. Figure 27 illustrates the thermal response extracted when the IR camera was oriented at 70°, 45°, 30°, and 15° from a perpendicular position with respect to the specimen. From the results, shown in Figure 27, the TSA response remains fairly constant when the camera's angle of view is less than 70°. Hence, it is recommended that the camera angle of orientation should not be greater than 45°.

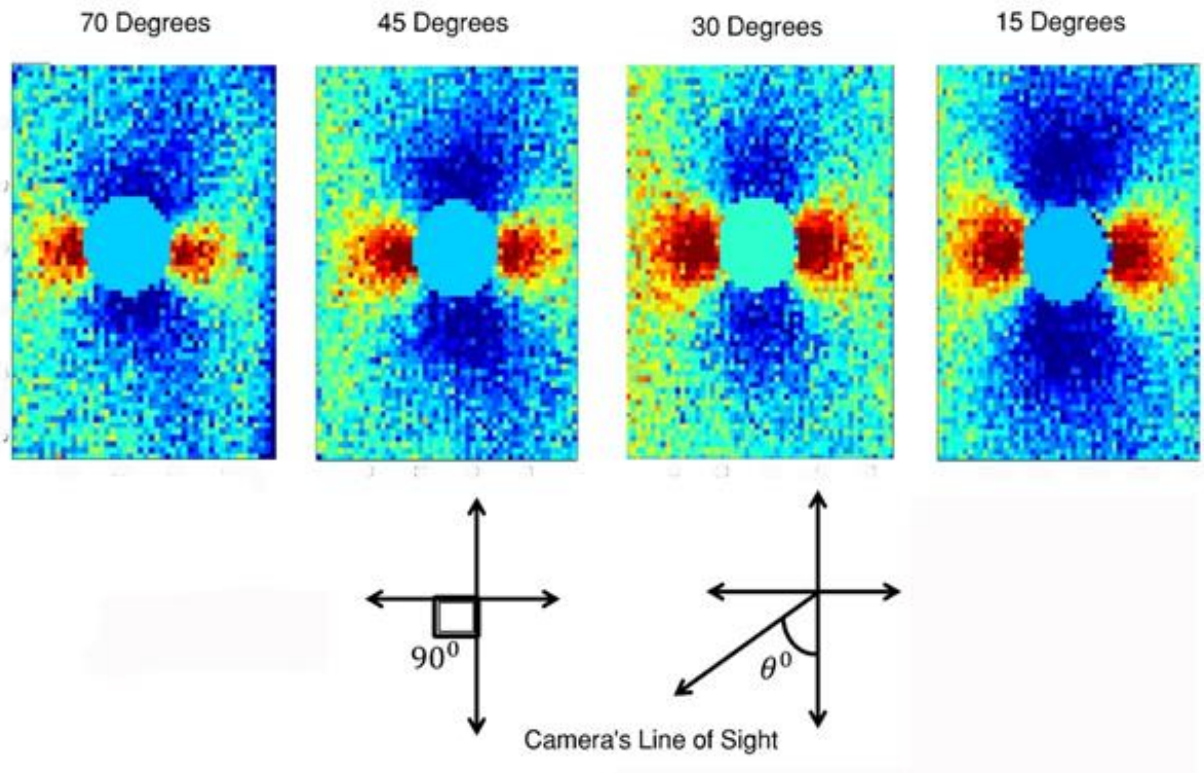

Figure 27. TSA Response From Camera Oriented at 70°, 45°, 30°, and 15°. Results obtained with total of 20 events in 10 seconds.

Fatigue Crack Detection

In the presence of a crack or discontinuity, the TSA response is pronounced due to the high stress values and high stress gradients at the tip of the crack.

Experiment 6

A notch-in-plate specimen, shown in Figure 28, was used to test the feasibility of using TSA to detect fatigue cracks. The nominal cross-sectional dimensions of the test specimen were identical to those of the hole-in-plate specimen. A fatigue crack was generated at the notch by cyclically loading the specimen. The fatigue crack was identified after about 800,000 cycles. A more pronounced crack was seen after a total of 1,010,000 cycles. Figure 29 shows the TSA response obtained by applying different types of loading events on this specimen. It is clear that the presence of a fatigue crack produces a thermoelastic response and high image contrast during high stress events, as defined by the event classifications found in Table 1.

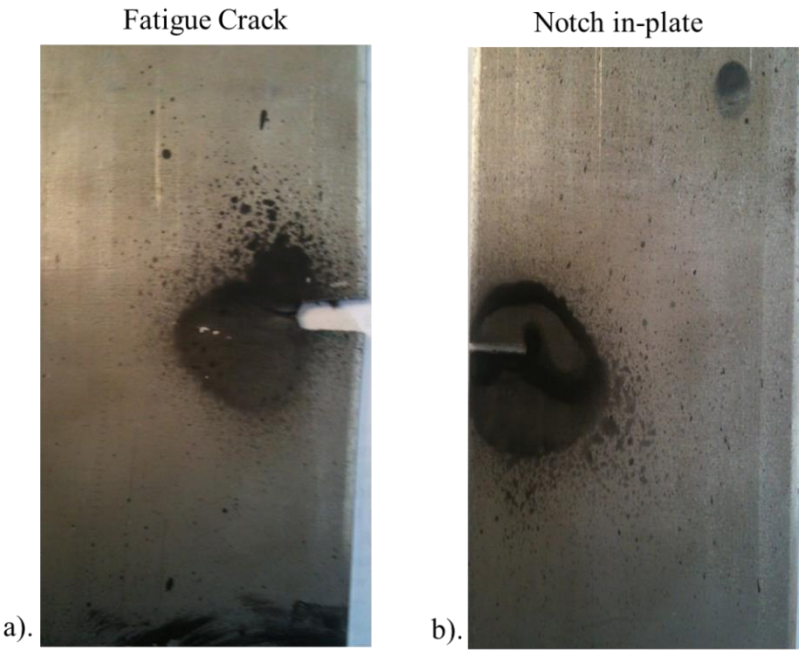

Figure 28. Notch-in-Plate Specimens With a) Growing Fatigue Crack and b) No Crack

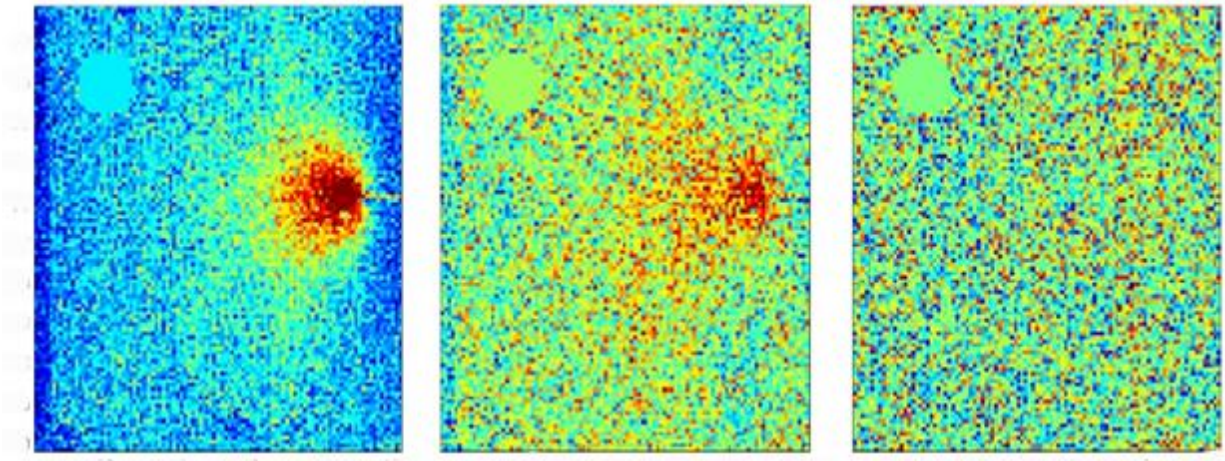

Figure 29. TSA Response of Notch in-Plate Specimen With a Growing Fatigue Crack at the Tip of the Notch Under Loads (From Left to Right) of 3.5 kip (14 ksi), 2.5 kip (10 ksi) and 1.25 kip (5 ksi)

Experiment 7

The final experiment conducted tested the feasibility of using the TSA technology to detect fatigue cracks under paint. A crack was grown from a through notch in the specimen. This produced two fatigue cracks, each propagating from the ends of the notch. The results of this experiment are shown in Figure 30. The experiment confirmed that TSA could be used for detecting cracks under paint. However, it is speculated that results may be sensitive to untested factors, such as the type of paint or thickness of paint.

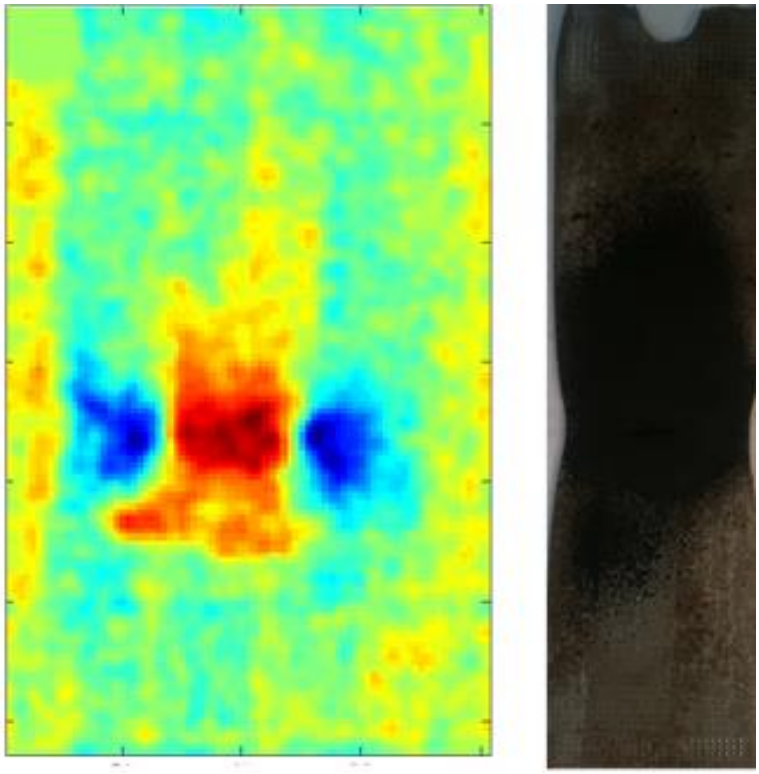

Figure 30. TSA of Specimen With Horizontal Cracks Under Black Paint. The blue hued portions of the image are due to high tensile stresses at crack tips.

Field Testing and Evaluation

The IR-TSA system was deployed on a steel bridge, shown in Figure 11, to collect IR response data with data acquisition triggered by random vehicular events over time. The goal of field-testing was to evaluate the feasibility of deploying the IR-TSA system on a bridge and extracting stress concentration images of fatigue prone details.

Fatigue Prone Detail

The bridge selected as the subject for the field testing had a history of fatigue cracks at several details. The specific detail evaluated with the TSA-IR system is shown in Figure 31.

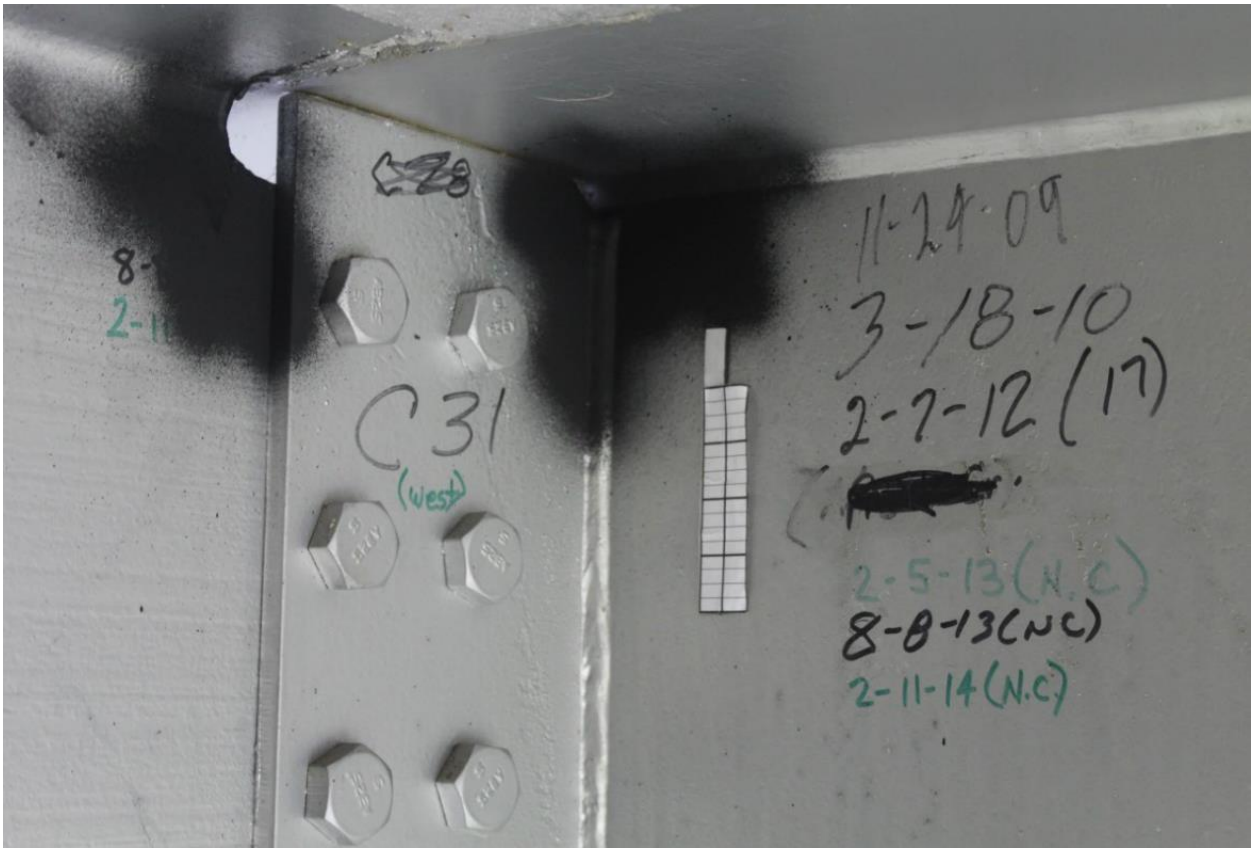

Figure 31. Floor-Beam Web Connection on I-64 Maury River Bridge

The system was field tested on the I-64 Maury River Bridge. It was deployed to measure full field stress at a detail where fatigue cracks have been a problem. The specific location tested, Figure 31, was a floor beam to girder connection at the interior of the fascia girder on the south side of the Eastbound Bridge.

Fatigue cracks exist at the cope of the floor beam and in the web at the termination of the connection plate weld. The crack at the floor beam cope initiates in a reentrant imperfection in the flame cut cope and extends approximately 1 inch into the web of the floor beam. The crack in the girder web is u shaped and is due to out of plane distortion in the web gap, both locations were covered with a layer of flat black paint, in preparation for use of the TSA-IR system.

The TSA-IR System was deployed on the bridge as shown in Figure 12. A clamp on strain gage was attached to the bottom flange of the floor beam. The floor beam deflects when a heavy truck travels over the bridge. The strain gage is shown in Figure 32. The strain gage was connected to one of the low level data acquisition channels available on the field computer. The field computer is shown in Figure 33.

Figure 32. Clamp-on Strain Gage

Figure 33. Field Computer

Data Processing and Analysis

The strain gage signal was observed as trucks passed over the bridge. A typical signal trace is shown in Figure 34.

Raw sample outputs from both the strain transducer and the microbolometer IR camera following an event that triggered the IR-TSA system are shown in Figures 34 and 35. The output from the strain transducer was filtered through a low-pass filter to remove noise. The maximum stress levels recorded on the bridge by the strain transducer ranged between 0.02 and 0.07 mV/V.

The trigger level was set at 0.025 mV/V with pre-trigger data acquisition time set to 1 second and post trigger time set to 6 seconds. A total of 13 heavy truck events were captured by the TSA-IR System. The acquired data from the camera and the reference sensor from all 13 events were post-processed, using the time-frequency domain lock-in algorithm described in the Methodology Section. The result of processing the data acquired is shown in Figure 36.

As seen in Figure 36, the IR-TSA system detected a high stress concentration at the termination of the weld on the connection plate bolted to the floor beam during actual traffic loading conditions. Fatigue cracking of this detail may be initiated in the future in response to the stress concentration detected. Modifying this detail could help in preventing or arresting fatigue cracking at this detail. The vertical lines on the processed image are due to the shaking of the camera as vehicles passed over the bridge. Currently, motion stabilizers have not been developed for the system.

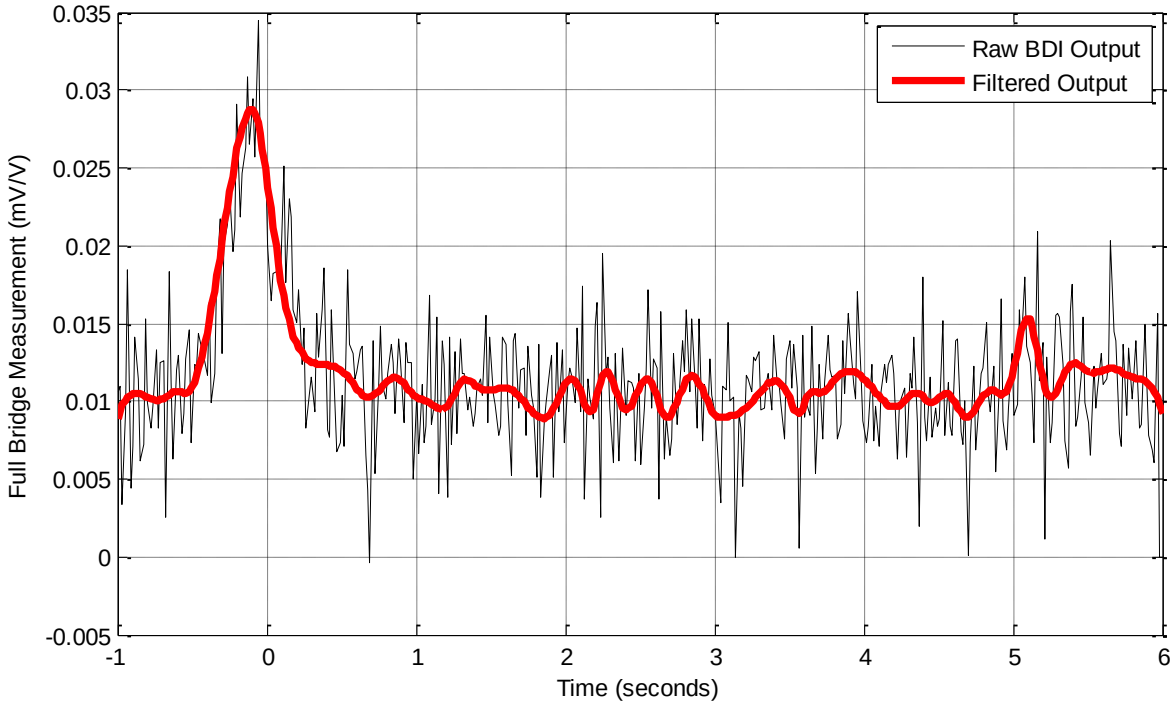

Figure 34. Sample Reference Signal Acquired Using Clamp-on Strain Gage

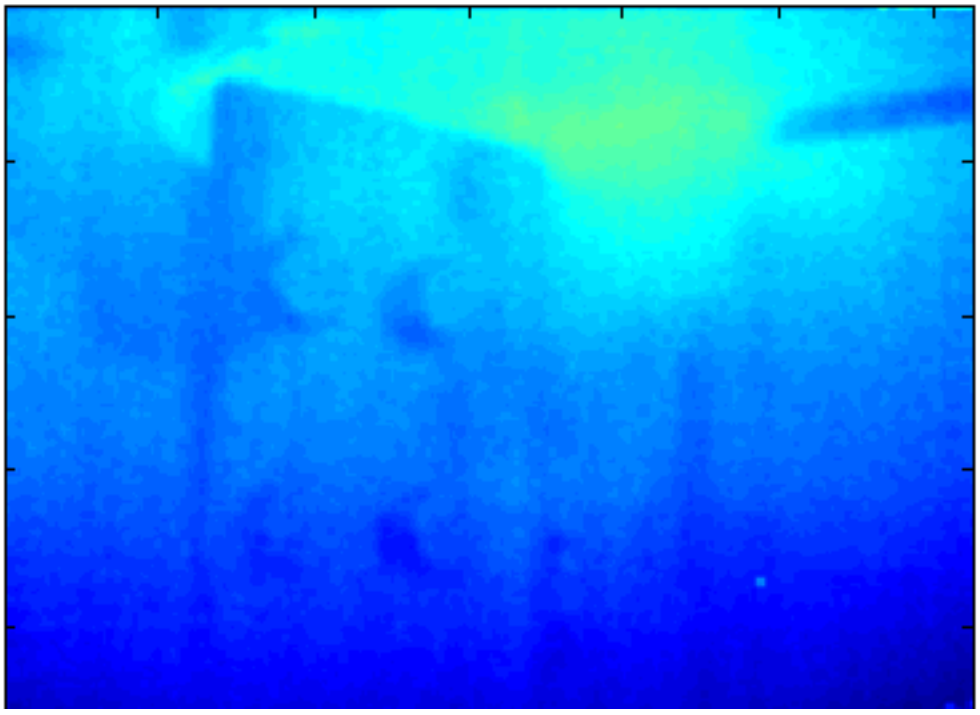

Figure 35. Raw Infrared Image of Fatigue Prone Detail

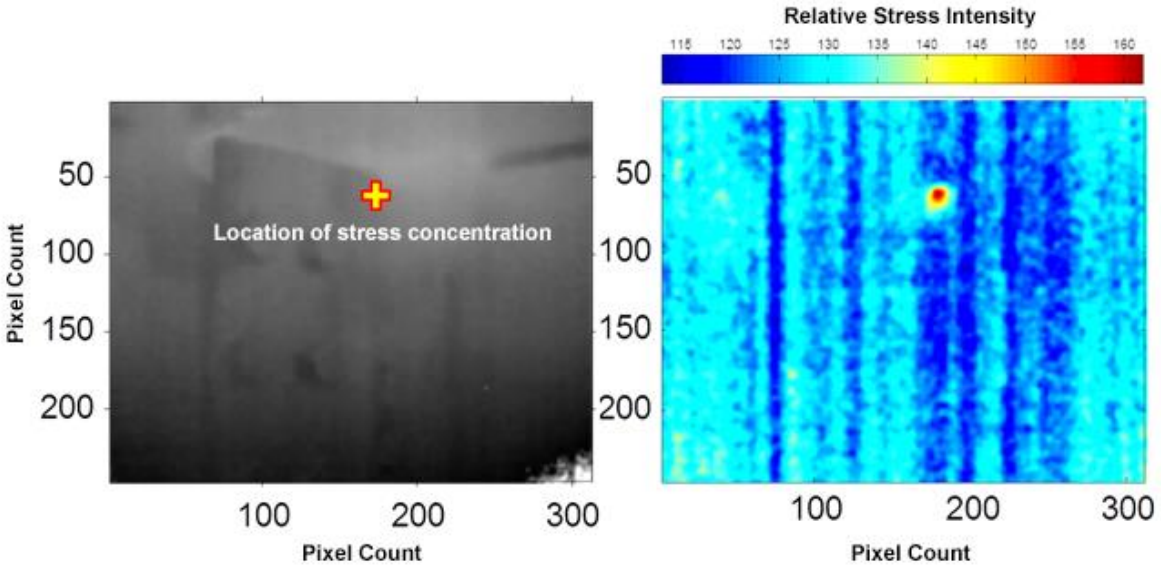

Figure 36. Fatigue-Prone Detail Showing a) Reference Image, and b) Thermoelastic Response of Detail

To increase confidence in these results, a 3D FEM of the detail under typical loading was built. The results of that FEM are shown in Figure 37. The FEM replicated the observed stress concentration pattern, providing a high confidence that the measured results were accurate.

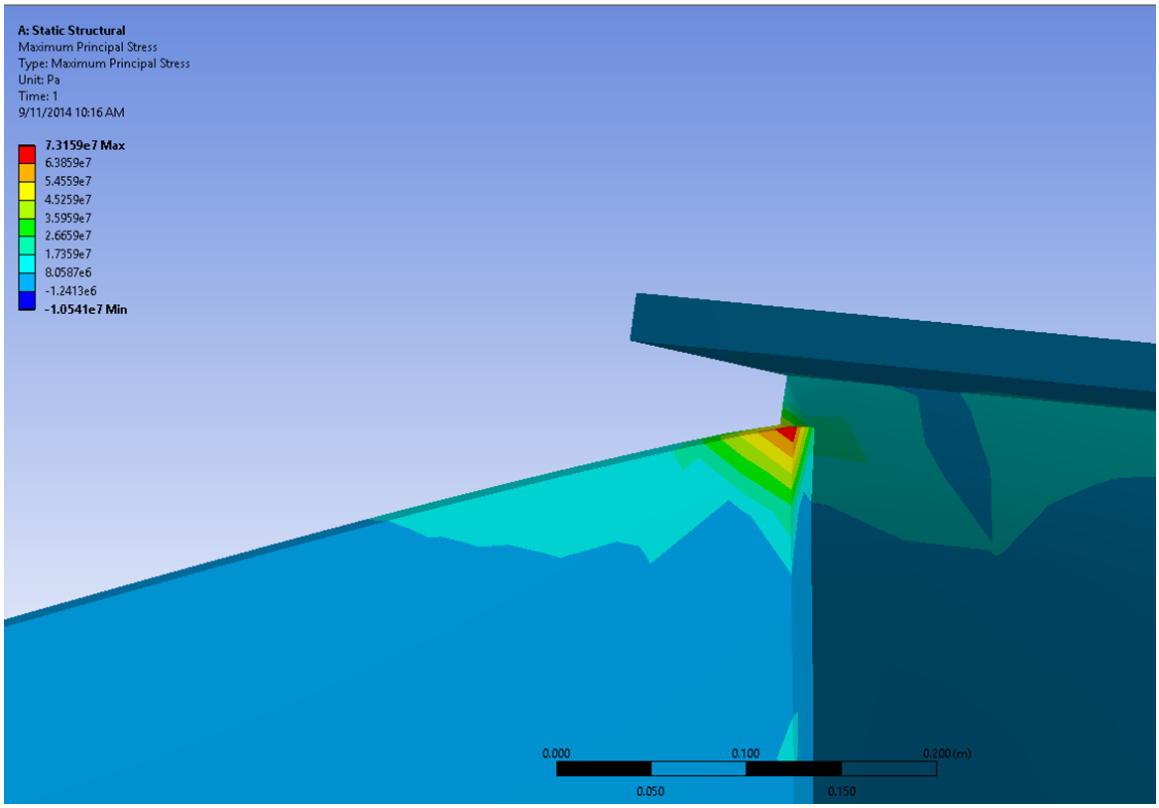

Figure 37. Stresses Due to Floor Beam Deflection at Connection Plate

DISCUSSION

This report documents the development, validation and application of a novel IR-TSA system for in situ evaluation of stress fields in the vicinity of fatigue-prone details on highway bridges. The IR-TSA system is based on a relatively low-cost microbolometer thermal imager, a dedicated computer unit for triggering data acquisition and specialized signal post- processing algorithms capable of extracting small changes in surface temperature associated with dynamic loading events. The system was validated by qualitative and quantitative comparisons between laboratory and simulated measurements. A laboratory and an experimental field study were conducted to evaluate the application of the IR-TSA system for detecting and monitoring fatigue cracks in steel specimens and in service bridges. Based on laboratory experiments, it was shown that at moderate to high stress levels, TSA could be used to image stress concentrations at the tip of fatigue cracks due to random loading events. Also, the system is fully applicable to the measurement and visualization of stress concentrations present at fatigue-prone details on highway bridges subject random truck loading. The TSA-IR System can also be applied to any metal structure with fatigue prone details, such as sign supports and light poles.

The output of the current system provides a visualization of the stress concentrations at fatigue prone details. A quantitative description of stress levels at a detail could be very useful for decision-making and comparative studies. One other important challenge to consider in the future is how to stabilize the IR camera or compensate for camera movement when located in dynamic environments.

CONCLUSIONS

- *The thermoelastic stress phenomena of solid materials can be exploited to determine locations of elevated stress in structural components subject to dynamic load applications.*

- *A relatively low-cost, microbolometer-based IR camera can be used in situ to capture thermoelastic stress-induced heat emissions from in-service structures.*

- *TSA can be used with events that are random in frequency and magnitude by correlating IR image data to a reference signal, such as associated strain data.*

- *By using time-and-frequency domain lock-in techniques, TSA can extract useful information about stress distributions from series of IR images containing high levels of noise relative to the signal of interest.*

- *The IR-TSA system developed under this project is available for use by VDOT district structure and bridge personnel to evaluate fatigue-prone details on existing bridges.*

RECOMMENDATIONS

1. *VDOT's Structure and Bridge Division should employ the TSA system developed in this study to assess the presence and location of high stress concentrations in steel or other metal structures.*

2. *The Virginia Transportation Research Council (VTRC) should support an implementation project to conduct field trials of the TSA system, with emphasis on refining the field-readiness and ease of use.*

3. *VTRC should employ the TSA system to evaluate fatigue and fatigue cracking on ancillary structures, such as sign supports and signal supports.*

BENEFITS AND IMPLEMENTATION

Benefits

The cost of a typical fatigue retrofit on an in-service bridge is estimated to be about $65,000, as itemized in Table 3.

The TSA system can be used to perform the following tasks:

- Locate/confirm high stress locations on in-service bridges and other structures.
- Confirm existence and extent of fatigue cracks on existing details.
- Evaluate effectiveness of retrofit and repair actions.

Table 3. Estimated Costs of Typical Fatigue Retrofits on a Bridge

Item Description	Cost
Mobilization	$10,000
Traffic Control	$25,000
Bridge Access Equipment Rental	$5,000
Retrofit Materials and Labor $2,500 per site (assume 10 sites)	$25,000
Total	$65,000

Normal practice is not to evaluate existing structures for high stress locations unless evidence of fatigue damage is observed. This is most often the observation of a fatigue crack during a routine bridge inspection. Once a crack has been observed, an engineering evaluation is usually conducted to determine the cause of the crack and to recommend corrective actions. This can be challenging because, as documented in this report, the stress fields at fatigue prone bridge details can be geometrically complex and the loading conditions leading to fatigue damage are random and transient. It can also be difficult to determine the extent of fatigue cracks on existing bridges due to difficult access, low visibility and painted surfaces. It is not uncommon to perform a fatigue retrofit, such as drilling a stop hole at the tip of the existing crack, and later find that the retrofit was ineffective. Multiple hole drilling retrofits are not unusual, as illustrated in Figure 38.

The use of the TSA system can improve the evaluation of existing fatigue cracks and ensure that whatever repair or retrofit actions are performed are effective. If the use of the TSA system eliminates the need for subsequent repairs, then a savings of approximately $65,000 will accrue in each instance. This does not include the indirect benefits to the travelling public and the improved reliability and safety of the bridges.

Figure 38. Multiple Holes Drilled at Fatigue Crack

Implementation

With regard to Recommendation 1, opportunities exist for VDOT's Structure and Bridge Division to further pilot and implement the TSA technology developed under this project. The following activities will be coordinated by the Assistant State Structure and Bridge Engineer for Maintenance and appropriate district bridge personnel over the next year:

- Field deployment on the I-64 Delta Frame EBL bridge to confirm the effectiveness of fatigue-reducing retrofit details that were installed as part of the ongoing rehabilitation project. Specific locations of high stress evaluated during this research project can be observed again, post-repair, to confirm effectiveness. Additional fatigue-prone details (e.g., at welds near stiffener-to-web or flange connections) can be monitored for a short period as well.

- Field trials in locations where fatigue cracks are to be (or have been) drilled out for fatigue crack arrest purposes, as well as those retrofitted with compression ring (i.e., StopCrackEX) for verification. The system can be used to observe stresses under live load immediately prior to, and then immediately following crack arrest application to verify the effectiveness of the retrofit. A parametric study of hole size and location for different fatigue cracks and modes of crack propagation is now possible with the TSA system, and may be explored.

- Publish guidance in the *Manual of the Structure and Bridge Division* for the practical use of TSA technology. Guidance will describe when and how to use TSA technology.

With regard to Recommendation 2, to augment the current capabilities of the prototype system, VTRC may purchase a new battery power supply for the TSA system. Fuchs Consulting Inc. has continued development of this product and has a new battery power supply that is smaller and provides power over a longer time than the battery used for the prototype system currently available to VTRC. If the technical review panel/implementation team supports further refinements of the system to increase efficiency and usefulness, VTRC may consider funding additional refinement activities, which may include:

- The addition of image stabilization to the post-processing performed on field images to improve the clarity and resolution of the TSA output

- Future research to provide quantitative stress values, as the current TSA system can visualize stress fields and useful information can be extracted, but is based on qualitative comparisons.

With regard to Recommendation 3, VTRC will consider opportunities for field trials on typical aluminum luminaire or steel cantilever sign structures at locations where previous fatigue failures have occurred on similar structures (e.g., the pole-to-base plate weld of aluminum luminaire poles, or near hand holes on 895 luminaire poles) to assess stress concentrations under wind loading.

ACKNOWLEDGMENTS

The authors acknowledge the financial and technical support of VDOT and VTRC for this research. In particular, the assistance of the technical review panel consisting of Rex Pearce, Staunton District Bridge Engineer (champion); Adam Matteo, Assistant State Structure and Bridge Engineer; and Jeffrey Milton, Bridge Preservation Engineer, is acknowledged.

REFERENCES

Ciupa, R., and Rogalski, A. 1997. Performance Limitations of Photon and Thermal Infrared Detectors, *Opto-Electronics Review*, Volume 5, Issue 4. Oct 2003,

Diaz, F.A., Patterson, E.A., and Yates, J.R. (2013). Application of Thermoelastic Stress Analysis for the Experimental Evaluation of the Effective Stress Intensity Factor, *Frattura ed Integrita Strutturale*, Volume 25, July 2013, pp 109-116.

Dullieu-Barton, J.M. (1999). Introduction to Thermoelastic Stress Analysis, *Strain*, Volume 35, Issue 2.May 1999, pp 35-39

Emery, T.R. and Dulieu-Barton, J.M. (2010). Thermoelastic Stress Analysis of Damage Mechanisms in Composite Materials, *Composites Part A: Applied Science and Manufacturing*, Volume 41, Issue 12, December 2010, pp 1729-1742.

FLIR, *Cooled Versus Uncooled Cameras for Long Range Surveillance*, Technical Note 0005, FLIR® Commercial Systems,

Freuhmann, R.K., Dulieu-Barton, J.M., and Quinn, S. Thermoelastic Stress and Damage Analysis Using Transient Loading. *Experimental Mechanics*, Volume 50, Issue 7, September 2010, pp 1075-1086.

Friis, E.A., Cookie, F.W., McQueen, D.A. and Henning, C.E. (1993). Thermoelastic Stress Analysis of the Human Patella: Effect of Bone Block Removal and Patellar Prosthesis, *Journal of Biomechanics*, Volume 26, Issue 3, March 1993, pp 352-362.

Greenee, R.J., Patterson, E.A., and Rowlands, R.E. (2008). Thermoelastic Stress Analysis, *Springer Handbook of Experimental Solid Mechanics*. W.N. Sharpe (ED), Springer Science and Business Media, LLC New York, 2008

Haldorsen, L.M., Thermoelastic Stress Analysis System Developed for Industrial Applications, Ph.D. dissertation, 1998, Aalborg University, Aalborg.

Harwood, N., and Cummings, W.M. Thermoelastic Stress Analysis, IOP Publishing Ltd, Bristol, England, 1991.

Johnson, S.M., Infrared Thermography and Thermoelastic Stress Analysis of Composite Materials and Structural systems, M.S. Thesis, Georgia Institute of Technology. 2006.

Kantner, M., Evaluating Fatigue Cracks in Steel Bridges with Thermoelastic Stress Analysis. MS Thesis, University of Virginia, .

Mandeno, W.L. and Sarraf, R.E., Protective Coatings for Steel Bridges: A Guide for Bridge and Maintenance Engineers, New Zealand Transport Agency 2014. www.nzta.govt.nz/resources/protective-coatings-steel-bridges/docs/nzta-protective-coatings-for-steel-bridges.pdf.

Myers, J.J., and Washer, G., Structural Steel Coatings for Corrosion Mitigation. Missouri Department of Transportation, 2010, www.library.modot.mo.gov/RDT/reports/TRyy0911/or11006rpt.pdf.

Patki, A.S., and Pratterson, E.A., Thermoelastic Stress Analysis of Fatigue Cracks Subject to Overloads, *Fatigue and Fracture of Engineering Materials and Structures*, Volume 33, Issue 7, July 2010, pp 809-821.

Pilkey, W.D. and Pilkey, D.F., Peterson's Stress Concentration Factors (2nd Edition). John Wiley & Sons Inc, New York, 2008.

Rajic, N. and Rowlands, D., Thermoelastic Stress Analysis with a Compact Low-Cost Microbolometer System, *Quantitative Infrared Thermography Journa*l, Volume 10, Issue 2, June 2013, pp 135-158.

Rogalski, A., Infrared Detectors: an Overview, *Infrared Physics and Technology*. Volume 43, Issues 3-5, June 2002, pp 187-210.

Shah, S., Bougherara, H., Schemitsch, E.H., and Zdero, R., Biomechanical Stress Maps of an Artificial Femur Obtained Using a New Infrared Thermography Technique Validated by Strain Gages, *Medical Engineering and Physics*, Volume 34, Issue 10, March 2012, pp 1496-1502.

Timoshenko, S., and Goodier, J., Theory of Elasticity (2nd Edition), McGraw-Hill Book Company, Inc., New York, 1951.

Wei, B., Thermoelastic Stress Analysis Techniques for Mixed Mode Fracture and Stochastic Fatigue of Composite Materials, Ph.D. Dissertation, Georgia Institute of Technology, 2008.

Zanetti, E.M., Cristina, B., and Audenino, A.L. Human Pelvis Loading Rig for Static and Dynamic Stress Analysis, *Acta of Bioengineering and Biomechanics,* Volume 14, Number 2, June 2012, pp 61-66.

Zanetti, E.M., Musso, and Audenino, A.L., Thermoelastic Stress Analysis by Means of a Standard Thermocamera, *Experimental Techniques*, Volume 31, Issue 2, February 2007 pp 42-50.

APPENDIX

MATLAB PSEUDO-CODE DESCRIPTIONS OF DATA PROCESSING ALGORITHMS

Pseudo-Code: Lock-in Algorithm

The lock-in algorithm extracts temperature variations correlated to the loading history of the specimen. The algorithm is implemented in the frequency domain; hence correlation is replaced by convolution. The pseudo-code below is implemented by m-file **lock-in.m** in MATLAB.

Let $\boldsymbol{y(t)}$ be the reference signal sampled simultaneously with $\boldsymbol{f(x,y,t)}$, a sequence of infrared images of the detail.

Where:

$\boldsymbol{t}$ is the total duration (pre and post trigger) of data acquisition
$\boldsymbol{x = 1}$: **M**, where **M** the number of rows in each frame and
$\boldsymbol{y = 1}$: **N**, where **N** is the number of columns in each frame.

1. Transform reference signal $\boldsymbol{y(t)}$ from time into a frequency-domain and take a derivative of the signal in the frequency domain.

$$\boldsymbol{Y(\omega) = \frac{\delta}{\delta \omega} \mathbf{FFT}(y(t))}$$

2. Transform each pixel $\boldsymbol{f_{mn}(x^m, y^n, t)}$, in the infrared data $\boldsymbol{f(x,y,t)}$ also into frequency domain.

$$\boldsymbol{F_{mn}(\omega) = \mathbf{FFT}(f_{mn}(x^m, y^n, t))}$$

3. Convolve each transformed pixel with the reference signal in step 1 and apply an inverse Fourier transform ($\boldsymbol{\mathcal{F}^{-1}}$) to return result from frequency domain into time domain.

$$\begin{aligned} \boldsymbol{g_{mn}(t)} &= \boldsymbol{\mathcal{F}^{-1}\{conv[Y(\omega), F_{mn}(\omega)]\}} \\ &= \boldsymbol{\mathcal{F}^{-1}\{Y(\omega) * F_{mn}(\omega)\}} \end{aligned}$$

4. Calculate the mean of $\boldsymbol{g(t)}$ as the processed output of pixel $\boldsymbol{(m,n)}$.

$$\boldsymbol{P(m,n) = \frac{1}{T} \sum_{t=1}^{T} |g_{mn}(t)|}$$

$\boldsymbol{P(m,n)}$ is the processed image.

Pseudo-Code: Image Smoothing

Contour plotting of thermoelastic responses may require smoothening of the processed output. The pseudo code below uses a Gaussian filter to illustrate the smoothening processing.
The m-file **fft_image.m** implements this pseudo code in MATLAB.

1. Select a 2D low-pass filter (preferably Gaussian) and take its Fourier transform

$$\boldsymbol{H(\omega_x, \omega_y) = \mathrm{FFT\_2D(filter)}}$$

2. Similarly take a Fourier transform of the processed output image.

$$\boldsymbol{F(\omega_x, \omega_y) = \mathrm{FFT\_2D}(f(x, y))}$$

3. Convolve results in step 1 and 2 and take an inverse Fourier transform ($\boldsymbol{\mathcal{F}^{-1}}$) to return result from frequency domain into time domain.

$$\boldsymbol{g(x, y) = (\mathcal{F}^{-1}\{H(\omega_x, \omega_y) .* F(\omega_x, \omega_y)\})}$$

Pseudo-Code: Phase Shifting

Phase shifting is used to find the optimal synchrony between the load and the temperature variations.
The m-file **phase_shift.m** implements this pseudo code in MATLAB.

1. Select a range of phase values between zero and pi;

2. Take a Fourier transform of the reference signal.

$$\boldsymbol{Y(\omega) = \mathrm{FFT}(y(t))}$$

3. Shift the phase of the reference signal by multiplying the Fourier transformed reference signal with a complex conjugate of the phase values. Take an inverse Fourier transform to return data into time domain.

$$\boldsymbol{g(x, y) = (\mathcal{F}^{-1}\{Y(\omega) .* exp(i * phase)\})}$$